Table 2 *Laboratory and neuroimaging findings of eight patients with MM2-type sCJD*

	EEG			CSF		Abnormal signals on MRI*				Reduction of CBF or hypometabolism			
Patient no.	Slowing	PSWCs	DD, mo	14-3-3	DD, mo	CO	BG	TH	DD, mo	CO	BG	TH	DD, mo
1	+	−	13	+	9	+	−	−	7	+	−	−	9
2	+	+	27	+	16	+	−	−	16	+	−	−	16
3	+	−	11	±	4	+	−	−	4	+	−	+	4
4	+	−	25	NA		NA				+	−	+	16
5	+	−	42	NA		NA				+	−	+	12
6	+	+	36	NA		−	−	−	58	+	−	+	37
7	+	−	9	+	9	−	−	−	13	NA			
8	+	−	7	±	7	−	−	−	7	+	−	+	7

sCJD = sporadic Creutzfeldt–Jakob disease; CBF = cerebral blood flow; PSWCs = periodic sharp-wave complexes; DD = disease duration at time point when each examination showed the following results: PSWCs on EEG, positive 14-3-3 protein in CSF, abnormal signals on MRI, and reduction of CBF on SPECT or hypometabolism on [^{18}F]2-fluoro-2-deoxy-D-glucose PET or at the time when the last examination was performed if the examinations revealed negative results throughout the clinical course; CO = cortex; BG = basal ganglia; TH = thalamus.

* We judge that abnormal signals are positive on MRI when they are shown on any sequence, such as T1-weighted, T2-weighted, diffusion-weighted, and fluid-attenuated inversion recovery images.

duction of the CBF in the bilateral parietal and temporal cortices (figure 2A). CSF examination revealed an increased level of 14-3-3 protein (28 ng/mL [normal <20 ng/mL]). Although the clinical criteria of sCJD[20] were not fulfilled because of the scarcity of neurologic and EEG abnormalities, CJD was suspected on the basis of MRI and CSF findings.

Twenty-seven months after the onset, the EEG showed PSWCs. Cortical hyperintensity signals on DWI were found to extend to the bilateral frontal regions. ^{99m}Tc-ECD SPECT showed diffuse severe reduction of CBF except in the cerebellum, basal ganglia, and thalamus. To confirm the diagnosis of CJD for participation in a clinical trial of pentosan polysulfate, brain biopsy of the right frontal lobe was performed with her family's consent 28 months after the onset. The patient developed myoclonic movement involving the bilateral hands and was alive 30 months after the onset.

Patient 3. A 65-year-old man developed unsteadiness with a tendency to fall to the left side. Three months after the onset, he showed gait disturbance and dysarthria.

Neurologic examination 4 months after the onset revealed slurred dysarthria, clumsiness of the left upper and lower extremities, and dementia. The EEG was normal. The CSF level of 14-3-3 protein was equivocal. MRI showed gyriform hyperintensity in the bilateral frontal, temporal, parietal, and occipital cortices on DWI. FDG-PET of the brain showed diffuse hypometabolism in the bilateral thalamus and cortices. CJD was suspected as an initial diagnosis.

Thereafter, the patient's symptoms rapidly progressed; he became bedridden and could not communicate 5 months after the onset. Myoclonus of the extremities developed 9 months after the onset. Eleven months after the onset, cortical lesions with hyperintense signals on DWI extended more widely than in the previous study and revealed diffuse, mild atrophy. EEG revealed diffuse slowing without PSWCs. The CSF level of 14-3-3 protein was still equivocal. The patient fell into akinetic mutism 13 months after the onset. He died 14 months after the onset and was autopsied.

Patient 8. A 58-year-old man developed progressive dementia. He showed unsteady gait 5 months after the onset and myoclonic movement in all limbs 6 months after the onset.

Neurologic examination 7 months after the onset revealed dementia, cerebellar ataxia, myoclonic jerking, and exaggerated deep tendon reflexes in all the extremities. Brain MRI, including DWI, and EEG were normal (see figure 1, C and D). CBF-SPECT using ^{99m}Tc-ECD revealed reduction of the CBF in the bilateral thalamus and cortices of the temporal and parietal lobes (see figure 2B). A CSF study disclosed a mild increase of protein concentration (44 mg/dL) and equivocal levels of 14-3-3 protein. The diagnosis was suspicion of Alzheimer disease (AD).

His symptoms gradually deteriorated. He also developed visual hallucinations and confusion 12 months after the onset. Thirteen months after the onset, he died and was autopsied.

PrP *gene analysis.* Analysis of the *PrP* gene revealed no mutation in any of the eight patients. The polymorphic codons showed methionine homozygosity at codon 129 and glutamic acid homozygosity at codon 219 in all the patients.

Neuropathology. Neuropathologically, the biopsy samples from the right frontal cortex of Patients 1 and 2 showed similar pathologic findings: prominent spongiform changes, including large vacuoles, with gliosis, and diffuse granular PrP immunostaining of synaptic type with a perivacuolar pattern.

Autopsies were performed in Patients 3 to 8. The neuropathologic findings of Patients 4 to 8 were similar. Severe neuronal loss and gliosis, but no spongiform changes, were observed in the nuclei of the medial thalamus as well as in the inferior olive. In the thalamus, PrP immunoreactivity was absent in all the patients. In the cerebral cortex, spongiform degeneration was absent in Patient 8 and limited to isolated foci in Patients 4 to 7 mainly in the frontal, pari-

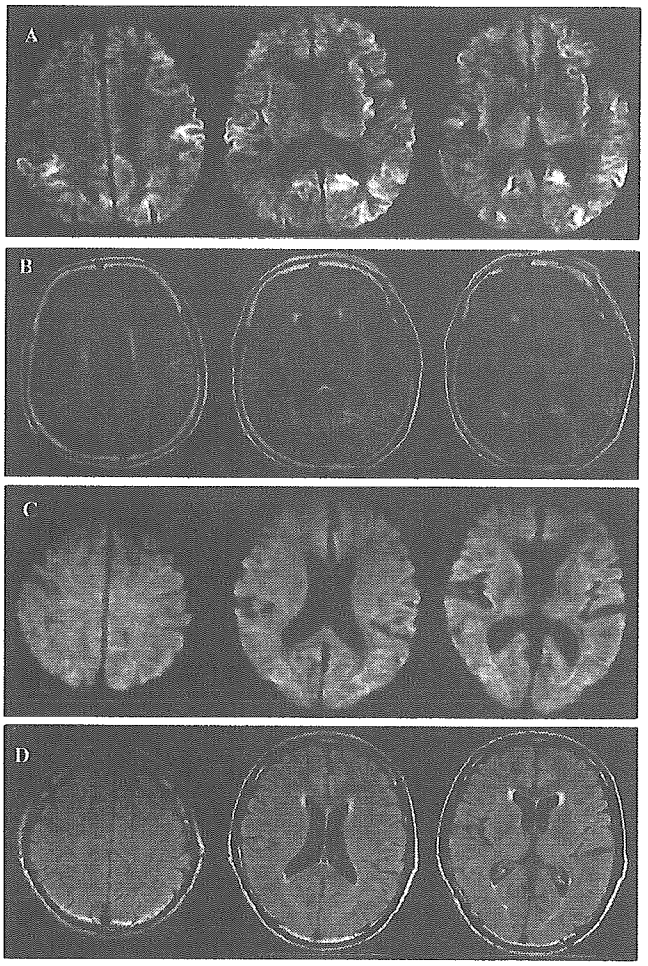

Figure 1. Brain MRI in Patient 2 at 16 months after the onset (A, B) and Patient 8 at 7 months after the onset (C, D). A and C are diffusion-weighted imaging (DWI), and B and D are fluid-attenuated inversion recovery (FLAIR) imaging. In Patient 2, DWI shows hyperintense signals in the bilateral frontal, parietal, and occipital cortices (A), and FLAIR imaging also shows slight hyperintensity signals within the cortical DWI lesions (B). In Patient 8, DWI and FLAIR imaging reveal no distinct abnormal signals in the brain (C, D).

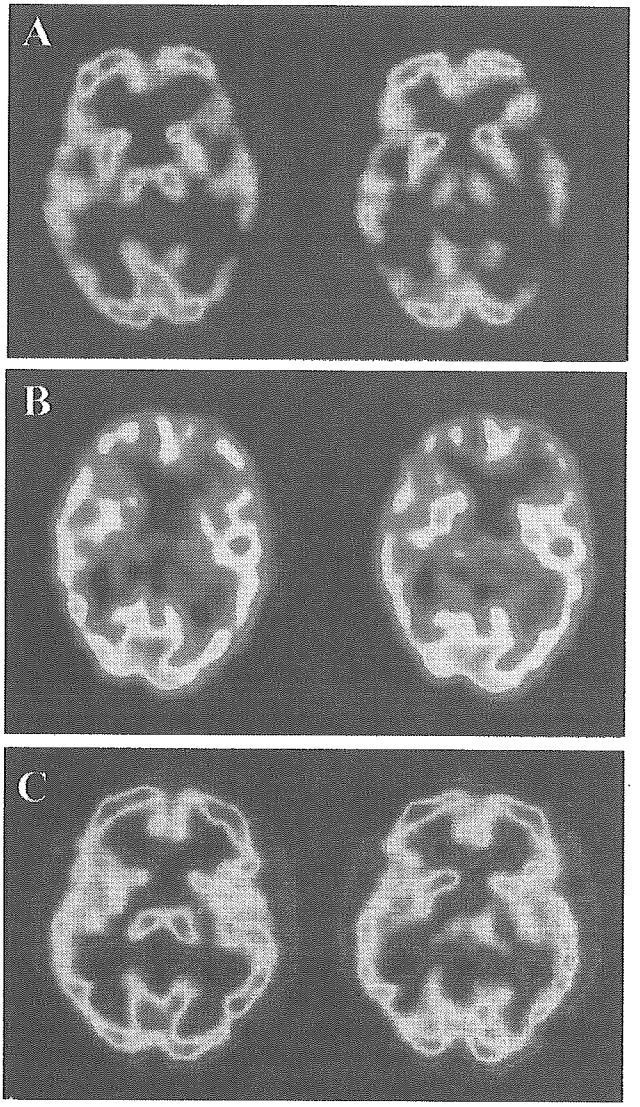

Figure 2. SPECT of cerebral blood flow (CBF) using ^{99m}Tc-ethyl cysteinate dimer in Patient 2 at 16 months after the onset (A), Patient 8 at 7 months after the onset (B), and a normal control subject who was a 67-year-old man without neurologic abnormality or cognitive decline (C). SPECT shows reduction of CBF in the bilateral temporal cortex in Patient 2 (A) and in the bilateral thalamus as well as the temporal cortex in Patient 8 (B) compared with the normal control subject (C).

etal, and temporal lobes, and PrP immunoreactivity was absent in Patients 5 and 8, whereas it was present with a sparse, coarse pattern in Patients 4, 6, and 7. In the subiculum, the neurons were well preserved, and spongiform changes were not evident in any of the patients. In the neostriatum, mild neuronal loss and gliosis were observed in all the patients. In the cerebellum, mild to moderate loss of Purkinje cells was observed, and PrP immunoreactivity was absent in Patients 4, 5, 7, and 8. In Patient 6, Purkinje cells were well preserved, but a small number of plaque-like PrP deposits were observed. In the cerebral white matter, mild or moderate myelin pallor was observed in Patients 4, 5, and 6.

Patient 3 showed the same severe lesions of the medial thalamus and the inferior olive as found in Patients 4 to 8, and PrP immunoreactivity was absent in the thalamus. Furthermore, the cerebral cortex in Patient 3 showed marked spongiform changes in all the layers with diffuse granular PrP staining. The other brain regions showed similar changes to those in Patients 4 to 8.

Western blot analysis. Western blot analysis of the brain samples from all the patients revealed PrP^{Sc} type 2A according to the classification of Parchi et al.[1,2] Compared with the amounts in Patients 1 to 3, only a small amount of PrP^{Sc} type 2A could be detected in Patients 4 to 8.

Discussion. *PrP* gene sequence and western blot analyses revealed that all eight of the patients studied here had MM2-type sCJD. As we analyzed PrP^{Sc} using brain tissue only from the frontal lobe, the

possibility of the coexistence of type 1 and type 2 of PrP^{Sc} in a single brain[3,21] cannot be ruled out. However, we consider it reasonable to classify our patients as having MM2-type sCJD, because the clinical and pathologic phenotypes of our patients were consistent with those of previously reported cases.[3,8,10] Neuropathologically, Patients 1 and 2 were classified as having the cortical form[3] and Patients 4 to 8 the thalamic form.[3] As Patient 3 presented with features of both the cortical and the thalamic forms, this case could be designated as the combined (corticothalamic) form. Because complete neuropathologic examination was not performed in Patients 1 and 2, the possibility that they had the combined form cannot be ruled out.

Patients 1 and 2 with the MM2 cortical form presented with late-onset, slowly progressive dementia (table 1). PSWCs on EEG were absent in the early stage (table 2). These features resembled those of previously reported MM2 cortical cases.[3] Our patients did not fulfill the clinical criteria for sCJD because of the scarcity of clinical symptoms.[20] Importantly, cortical hyperintensity signals on DWI (see table 2), which have been reported to be useful for diagnosis of sCJD,[19,22,23] easily led us to a possible diagnosis of CJD. The basal ganglia and thalamus in these cases showed no hyperintensity signals on MRI. Increased CSF levels of 14-3-3 protein supported the diagnosis (see table 2). As the MM2 cortical form frequently shows slowly progressive dementia without other neurologic abnormalities, AD and dementia with Levy bodies are important for differential diagnosis. Cortical hyperintensity signals on DWI are found in acute ischemic stroke,[23] herpes simplex meningoencephalitis,[22,23] posttraumatic contusion,[22,23] postictal change,[22] and MELAS (mitochondrial myopathy, encephalopathy, lactic acidosis, and stroke-like episodes)[24]; however, they are not observed in AD[25] or dementia with Lewy bodies.[19] We propose the following diagnostic criteria for MM2 cortical sCJD: 1) progressive dementia, 2) cortical hyperintensity signals on DWI, and 3) increased CSF 14-3-3 protein level, with exclusion of the other dementias, including other types of prion diseases. Other neuropsychiatric abnormalities than dementia or PSWCs on EEG are not necessarily required.

In the cases of MM2 thalamic form, the age at onset ranged from 30 to 71 years and the duration of the clinical course from 13 to 73 months (see table 1). Clinical manifestations included psychiatric symptoms, dementia, cerebellar ataxia, insomnia, and autonomic failure (see table 1). As for the outstanding features of FFI and SFI, insomnia was found in only one patient (Patient 4), and autonomic symptoms were found in three patients (Patients 4, 5, and 7). EEG showed no PSWCs except in one patient (Patient 6) who showed PSWCs in the very late stage (see table 2). These features resemble those of previously reported patients with MM2 thalamic[3] or SFI.[8,10] Brain MRI, including DWI, was almost normal in the MM2 thalamic patients except for brain atrophy or white matter changes in the late stage (see table 2). These features are consistent with previously those of reported patients with SFI.[8,10] In our study, of two patients tested for CSF 14-3-3 protein, one was positive and the other was equivocal (see table 2). In the literature, to our knowledge, there are reports of four patients with MM2 thalamic sCJD who have been examined for CSF 14-3-3 protein: The examination was positive in one[6] and negative in three.[7,8] Considering those reports together with our results, we cannot conclude that the CSF 14-3-3 protein is sensitive enough to diagnose MM2 thalamic sCJD. As the initial clinical diagnosis, progressive supranuclear palsy (PSP), spinocerebellar degeneration (SCD), or AD had been suspected (see table 1), indicating considerable difficulty in the clinical diagnosis of the MM2 thalamic form. However, our review of CBF-SPECT studies revealed characteristic findings of reduction of the CBF in the bilateral thalamus as well as the cerebral cortex from relatively early stages (see table 2). In previous reports of CBF-SPECT studies in CJD patients, reduction of CBF on visual inspection was found in various regions of the cerebral cortex but not in the thalamus.[26,27] There have been no reports about CBF-SPECT in MM2 thalamic sCJD. In FDG-PET studies, hypometabolism of the thalamus and cortex has been reported in a patient with SFI[10] or in some patients with FFI.[28,29] CBF and glucose metabolism in the thalamus are relatively preserved in AD.[30] In PSP, significant reduction of glucose metabolism is not detected in the thalamus but is detected in the frontal cortex by using region/occipital metabolic ratios.[31] In multiple system atrophy, a phenotype of sporadic SCD, reduction of the CBF in the thalamus was reported; however, significant reduction of the CBF was also detected in the dorsal putamen.[32] Our patients with MM2 thalamic sCJD showed no reduction of the CBF in the putamen (see figure 2B). Our results clearly indicate that reduction of CBF as well as hypometabolism in the bilateral thalamus, with their preservation in the putamen, would be a particularly useful diagnostic marker for the MM2 thalamic sCJD.

Interestingly, in the patient with the MM2 combined (corticothalamic) form (Patient 3), the neuroimaging studies showed features of both MM2 cortical and thalamic forms, that is, hyperintense signals in the cortex on DWI and thalamic hypometabolism on FDG-PET (see table 2), consistent with the pathologic findings in this patient.

Hyperintensity of the bilateral thalamus (the pulvinar sign) on MRI has been established to be a useful diagnostic marker for vCJD.[33,34] However, no abnormal signals in the pulvinar MRI can be detected in MM2-type sCJD, as shown in the current study and in previous reports.[8,10] A CBF-SPECT study in two patients with vCJD demonstrated widespread reduction of the CBF in the cerebral cortices but no obvious involvement of the thalami.[26] These CBF-SPECT features are different from those in

MM2 thalamic sCJD. Our results indicate the usefulness of neuroimaging studies in discrimination between vCJD and MM2-type sCJD.

References

1. Parchi P, Castellani R, Capellari S, et al. Molecular basis of phenotypic variability in sporadic Creutzfeldt–Jakob disease. Ann Neurol 1996;39: 767–778.
2. Parchi P, Capellari S, Chen SG, et al. Typing prion isoforms. Nature 1997;386:232–234.
3. Parchi P, Giese A, Capellari S, et al. Classification of sporadic Creutzfeldt–Jakob disease based on molecular and phenotypic analysis of 300 subjects. Ann Neurol 1999;46:224–233.
4. Collinge J, Sidle KC, Meads J, Ironside J, Hill AF. Molecular analysis of prion strain variation and the aetiology of "new variant" CJD. Nature 1996;383:685–690.
5. Hill AF, Joiner S, Wadsworth JD, et al. Molecular classification of sporadic Creutzfeldt–Jakob disease. Brain 2003;126:1333–1346.
6. Zerr I, Schulz-Schaeffer WJ, Giese A, et al. Current clinical diagnosis in Creutzfeldt–Jakob disease: identification of uncommon variants. Ann Neurol 2000;48:323–329.
7. Otto M, Wiltfang J, Cepek L, et al. Tau protein and 14-3-3 protein in the differential diagnosis of Creutzfeldt–Jakob disease. Neurology 2002; 58:192–197.
8. Parchi P, Capellari S, Chin S, et al. A subtype of sporadic prion disease mimicking fatal familial insomnia. Neurology 1999;52:1757–1763.
9. Castellani RJ, Colucci M, Xie Z, et al. Sensitivity of 14-3-3 protein test varies in subtypes of sporadic Creutzfeldt–Jakob disease. Neurology 2004;63:436–442.
10. Mastrianni JA, Nixon R, Layzer R, et al. Prion protein conformation in a patient with sporadic fatal insomnia. N Engl J Med 1999;340:1630–1638.
11. Yamashita M, Yamamoto T, Nishinaka K, Udaka F, Kameyama M, Kitamoto T. Severe brain atrophy in a case of thalamic variant of sporadic CJD with plaque-like PrP deposition. Neuropathology 2001;21: 138–143.
12. Will RG, Ironside JW, Zeidler M, et al. A new variant of Creutzfeldt–Jakob disease in the UK. Lancet 1996;347:921–925.
13. Will RG, Zeidler M, Stewart GE, et al. Diagnosis of new variant Creutzfeldt–Jakob disease. Ann Neurol 2000;47:575–582.
14. Yamada M, Itoh Y, Fujigasaki H, et al. A missense mutation at codon 105 with codon 129 polymorphism of the prion protein gene in a new variant of Gerstmann–Sträussler–Scheinker disease. Neurology 1993; 43:2723–2724.
15. Kitamoto T, Ohta M, Doh-ura K, Hitoshi S, Terao Y, Tateishi J. Novel missense variants of prion protein in Creutzfeldt–Jakob disease or Gerstmann–Sträuslller syndrome. Biochem Biophys Res Commun 1993;191: 709–714.
16. Kitamoto T, Shin RW, Doh-ura K, et al. Abnormal isoform of prion protein accumulates in the synaptic structures of the central nervous system in patients with Creutzfeldt–Jakob disease. Am J Pathol 1992; 140:1285–1294.
17. Shimizu S, Hoshi K, Muramoto T, et al. Creutzfeldt–Jakob disease with florid-type plaques after cadaveric dura mater grafting. Arch Neurol 1999;56:357–362.
18. Kawasaki K, Wakabayashi K, Kawakami A, et al. Thalamic form of Creutzfeldt–Jakob disease or fatal insomnia? Report of a sporadic case with normal prion protein genotype. Acta Neuropathol 1997;93:317–322.
19. Shiga Y, Miyazawa K, Sato S, et al. Diffusion-weighted MRI abnormalities as an early diagnostic marker for Creutzfeldt–Jakob disease. Neurology 2004;63:443–449.
20. Masters CL, Harris JO, Gajdusek DC, Gibbs CJ Jr, Bernoulli C, Asher DM. Creutzfeldt–Jakob disease: patterns of worldwide occurrence and the significance of familial and sporadic clustering. Ann Neurol 1979;5: 177–188.
21. Puoti G, Giaccone G, Rossi G, Canciani B, Bugiani O, Tagliavini F. Sporadic Creutzfeldt–Jakob disease: co-occurrence of different types of PrP^{Sc} in the same brain. Neurology 1999;53:2173–2176.
22. Demaerel P, Sciot R, Robberecht W, et al. Accuracy of diffusion-weighted MR imaging in the diagnosis of sporadic Creutzfeldt–Jakob disease. J Neurol 2003;250:222–225.
23. Schaefer PW, Grant PE, Gonzalez RG. Diffusion-weighted MR imaging of the brain. Radiology 2000;217:331–345.
24. Kolb SJ, Costello F, Lee AG, et al. Distinguishing ischemic stroke from the stroke-like lesions of MELAS using apparent diffusion coefficient mapping. J Neurol Sci 2003;216:11–15.
25. Bozzao A, Floris R, Baviera ME, Apruzzese A, Simonetti G. Diffusion and perfusion MR imaging in cases of Alzheimer's disease: correlations with cortical atrophy and lesion load. AJNR Am J Neuroradiol 2001;22: 1030–1036.
26. de Silva R, Patterson J, Hadley D, Russell A, Turner M, Zeidler M. Single photon emission computed tomography in the identification of new variant Creutzfeldt–Jakob disease: case reports. Br Med J 1998; 316:593–594.
27. Matsuda M, Tabata K, Hattori T, Miki J, Ikeda S. Brain SPECT with ^{123}I-IMP for the early diagnosis of Creutzfeldt–Jakob disease. J Neurol Sci 2001;183:5–12.
28. Perani D, Cortelli P, Lucignani G, et al. [18F] FDG PET in fatal familial insomnia: the functional effects of thalamic lesions. Neurology 1993; 43:2565–2569.
29. Cortelli P, Perani D, Parchi P, et al. Cerebral metabolism in fatal familial insomnia: relation to duration, neuropathology, and distribution of protease-resistant prion protein. Neurology 1997;49:126–133.
30. Ishii K. Clinical application of positron emission tomography for diagnosis of dementia. Ann Nucl Med 2002;16:515–525.
31. Blin J, Baron JC, Dubois B, et al. Positron emission tomography study in progressive supranuclear palsy. Arch Neurol 1990;47:747–752.
32. Van Laere K, Santens P, Bosman T, De Reuck J, Mortelmans L, Dierckx R. Statistical parametric mapping of 99mTc-ECD SPECT in idiopathic Parkinson's disease and multiple system atrophy with predominant parkinsonian features: correlation with clinical parameters. J Nuc Med 2004;45:933–942.
33. Zeidler M, Sellar RJ, Collie DA, et al. The pulvinar sign on magnetic resonance imaging in variant Creutzfeldt–Jakob disease. Lancet 2000; 355:1412–1418.
34. Collie DA, Summers DM, Sellar RJ, et al. Diagnosing variant Creutzfeldt–Jakob disease with the pulvinar sign: MR imaging findings in 86 neuropathologically confirmed cases. AJNR Am J Neuroradiol 2003;24:1560–1569.

Independent accumulations of tau and amyloid β-protein in the human entorhinal cortex

T. Katsuno, BSC; M. Morishima-Kawashima, PhD; Y. Saito, MD; H. Yamanouchi, MD; S. Ishiura, PhD; S. Murayama, MD; and Y. Ihara, MD

Abstract—*Background:* Previous studies have repeatedly described that neurofibrillary tangles arise earlier than senile plaques (SPs) in the entorhinal cortex, but one study suggested that SPs, if present, enhance the former lesions. All of these studies were performed at the histologic or immunocytochemical level, which may not accurately reflect the actual levels of amyloid β-protein (Aβ) and tau. *Objective:* To determine whether there is significant interaction between Aβ and tau in the human entorhinal cortex with regard to the Braak stage. *Methods:* Biochemical studies were conducted on 50 brains from elderly people, who were mainly at Braak stages I to III. All the cases were examined neuropathologically and staged according to Braak and Braak. A small piece of brain tissue for each case was dissected from the anterior portion of the right entorhinal cortex. The amounts of tau and Aβ in the insoluble fraction of the tissue were quantified using western blotting. *Results:* The levels of tau and possibly Aβ42 in the entorhinal cortex appeared to rise steeply at approximately age 75. The levels of insoluble tau increased as the Braak stage increased from I to II; however, it had a tendency to remain between stages II and III. The levels of Aβ42 showed a small increase, whereas those of Aβ40 increased continuously as the Braak stage advanced. In contrast, the extent of Aβ42 accumulation increased with increasing Braak stage for SPs. There was no significant correlation between the levels of insoluble tau and Aβ42 in the entorhinal cortex. Even if Aβ did not accumulate to significant extents, substantial accumulation of insoluble tau occurred. *Conclusion:* Accumulations of tau and amyloid β-protein occur independently in the human entorhinal cortex.

NEUROLOGY 2005;64:687–692

The entorhinal cortex is located on the ventromedial surface of the temporal lobe and is associated with the amygdaloid complex anteriorly and up to the midlevel of the hippocampus posteriorly.[1] There are widespread reciprocal connections between the entorhinal cortex and many cortical, subcortical, and hippocampal areas.[2] Information from many cortical and subcortical areas converges on the entorhinal cortex, which serves as the gateway for sensory information to the hippocampus. The entorhinal cortex sends a robust projection from layer II neurons, the perforant path, to the hippocampus. It has, in turn, connections to layer V neurons, which project to the neocortex.

During aging, neurofibrillary tangles (NFTs) spread throughout the human brain following a distinct pattern, which was firmly established by studying a great number of unselected human brains at various ages.[3] In Braak stages I and II, NFTs are confined in the transentorhinal and entorhinal cortex (transentorhinal stages). Further involvement of adjacent limbic areas leads to stages III and IV (limbic stages), and finally, involvement of the isocortex leads to stages V and VI (cortical stages). It has been reported that stages I and II are barely associated with any clinical symptoms, whereas stages V and VI invariably meet the neuropathologic diagnostic criteria for Alzheimer disease (AD) and are usually associated with clinical dementia.[4] Some individuals with stage III may or may not show signs and symptoms of mild AD or mild cognitive impairment (MCI).[4,5] It seems that the progression from stages I and II to stage III takes decades and is presumably critical for developing AD.[6] MCI, characterized by easy forgetfulness, may be a prodromal syndrome prior to AD. Even in this initial clinical stage, it has been reported that the entorhinal cortex is already heavily affected; up to one-half of the layer II neurons are lost, according to unbiased stereologic studies.[7]

Thus, the entorhinal cortex is the most vulnerable to NFTs and neuronal loss and can also be affected, somewhat later, by senile plaques (SPs),[8] a situation similar to what occurs with the hippocampus.[9] Therefore, the amyloid cascade hypothesis, at least in its original form, cannot be applied to the hippocampus and entorhinal cortex in the general aged

From the Department of Neuropathology (Drs. Morishima-Kawashima and Ihara, T. Katsuno), Faculty of Medicine, and Department of Life Science (Dr. Ishiura), Graduate School of Arts and Science, University of Tokyo, and Departments of Neurology (Dr. Yamanouchi) and Neuropathology (Drs. Saito and Murayama), Tokyo Metropolitan Geriatric Hospital and Tokyo Metropolitan Geriatric Institute of Gerontology, Japan.

Supported by a grant-in-aid for Scientific Research on Priority Areas—Advanced Brain Science Project—from the Ministry of Education, Culture, Sports, Science, and Technology, Japan, and a grant-in-aid for Science Research (C) from the Japan Society for the Promotion of Science (JSPS), Japan.

Received June 9, 2004. Accepted in final form October 29, 2004.

Address correspondence and reprint requests to Dr. Y. Ihara, Department of Neuropathology, Faculty of Medicine, University of Tokyo, 7-3-1 Hongo, Bunkyo-ku, Tokyo 113-0033, Japan; e-mail: yihara@m.u-tokyo.ac.jp

population. However, one may claim that histologic or immunocytochemical quantification for NFTs and SPs may leave some ambiguities. For example, SPs appear only when amyloid β-protein 42 (Aβ42) accumulates to certain critical levels,[9] which may differ from region to region. In addition, extracellular NFTs, which characterize the entorhinal cortex, may not be accurately recorded owing to decreased silver uptake or loss of immunoreactivity with commonly used tau antibodies. In this study, we addressed this issue by biochemically quantifying the amounts of tau composing NFTs and Aβ composing SPs in the insoluble fraction of entorhinal cortex.

Methods. *Subjects and sampling.* The current study is based on autopsy cases (n = 50; 26 men, 24 women) from the Brain Bank at the Tokyo Metropolitan Institute of Gerontology (Itabashi, Tokyo, Japan). This research project was approved by the local ethical committees at the Faculty of Medicine, University of Tokyo, and the Tokyo Metropolitan Institute of Gerontology and Tokyo Metropolitan Geriatric Hospital. Most of the subjects were evaluated according to the Clinical Dementia Rating Scale. The ages at death ranged from 53 to 93 years (table). The majority of the brains came from an affiliated, community-based geriatric hospital (Tokyo Metropolitan Geriatric Hospital). They were neuropathologically examined and classified according to Braak staging: six stages for NFTs and four stages for SPs[3] (stage O is defined as no SPs). The whole brain, after removal of the brainstem and cerebellum, was cut into halves, and the left hemisphere was fixed in 20% buffered formalin. The right hemisphere was cut into 7-mm-thick slices and quickly frozen with powdered dry ice, after sampling the anterior hippocampus as recommended by Braak and Braak[3] and the neocortex and midbrain as reported by the Consortium to Establish a Registry for Alzheimer's Disease (CERAD).[10] The sampled tissues were fixed in 4% paraformaldehyde for 48 hours, embedded in paraffin, and served for staging. With the left hemisphere, a number of samples were taken from representative areas after fixation, according to CERAD[10] and the recommendations of Braak and Braak.[3] Sampled blocks were embedded in paraffin, serially sectioned at 6 μm thick, and processed for hematoxylin/eosin and Klüver–Barrera stains. Selected sections were subjected to Congo red and silver stains, including Gallyas–Braak, modified methenamine silver, and modified Bielschowsky stains. For immunocytochemistry, the sections were incubated with each appropriately diluted antibody, anti-Aβ11–28 (mouse IgG monoclonal antibody raised against Aβ11–28; IBL, Maebashi, Japan), or AT8, which recognizes phosphorylated Ser202/Thr205 of tau (Innogenetics, Temse, Belgium). The rest of the procedure was performed on an automated Ventana immunostainer (Ventana NX20; Ventana, Tucson, AZ).

Specimens (about 0.2 g) of the anterior portion of entorhinal cortex were dissected according to a standard textbook[1] on a cryostat at −30 °C from an appropriate, 7-mm-thick slice, which had been stored at −80 °C. Braak stages for NFTs and SPs and immunocytochemical data of the specimens are presented in the table. As we were concerned about how the entorhinal cortex begins to be affected during aging, the specimens were randomly collected mainly from stage I to III brains. Subjects affected with multiple infarcts or a large infarct and those with progressive supranuclear palsy or corticobasal degeneration were excluded. In addition, subjects showing innumerable grains, numerous tau-positive astrocytes, and severe degrees of cerebral amyloid angiopathy were excluded.

Antibodies and recombinant tau. The monoclonal antibodies against Aβ used for this study were BA27 (highly specific for Aβ40) and BC05 (specific for Aβ42).[11] Pool-2 was raised against residues 299 to 385 of tau,[12] which contained the microtubule-binding domains. HT7 (Innogenetics, Gent, Belgium) and iD387 were described previously.[13,14] Paired helical filament-1 (PHF1), AT100 (Innogenetics, Gent, Belgium), AP422,[15] and anti-tau, phospho-specific (Ser262) (Calbiochem, San Diego, CA), were used for phosphorylation-dependent antibodies. A mixture of six isoforms of recombinant tau was used as the authentic tau for the quantification of NFTs. *Escherichia coli* expression and purification of recombinant tau were conducted as described.[14]

Sample preparation and western blotting. Frozen tissue samples were homogenized in 9 volumes of Tris–saline (TS) buffer containing a cocktail of protease inhibitors as described previously.[13,14] The homogenates were centrifuged at 265,000 *g* for 20 minutes, and the pellets were again homogenized in 9 volumes of TS buffer. One milliliter of the homogenates was used for quantification of tau and 0.5 mL for quantification of Aβ. For the preparation of Sarkosyl-insoluble tau (hereafter insoluble tau), 1 mL of homogenate was centrifuged at 265,000 *g* for 20 minutes. The pellet was homogenized in 0.9 mL of 1% Sarkosyl in TS buffer; after being kept on ice for 30 minutes, the suspension was centrifuged at 265,000 *g* for 20 minutes. The pellets (Sarkosyl-insoluble fraction) were washed twice with 1% Sarkosyl in TS buffer and solubilized by sonication in 250 μL of 2% sodium dodecyl sulfate (SDS) in 50 m*M* Tris-HCl (pH 7.6). Each fraction was mixed with equal volumes of 2× SDS sample buffer and subjected to western blotting,[14] with a defined amount of recombinant tau as an authentic control. Bound antibodies were detected by enhanced chemiluminescence (Amersham, Buckingham, UK). The amount of insoluble tau was quantified as follows. With use of the blot with pool-2, the signal intensities of the lane's total area, from the top to the bottom of gel, and an authentic recombinant tau were measured using a LAS-1000 Plus luminescent image analyzer (Fuji Film, Tokyo, Japan). The ratio of the signal intensities was calculated assuming the intensity of authentic recombinant tau as 100. This takes into account both the PHF-tau at about 68 kd and the tau-immunoreactive smear on the blot, the latter of which becomes dominant with increasing numbers of aged, especially ghost (extracellular) NFTs[13] (figure 1A). The microtubule-binding domains making up the fibrils are known to be highly resistant to proteases and were left as a smear after processing.[13] Thus, the relative score of Sarkosyl-insoluble tau can be regarded as a biochemical measure of NFTs (see figure 1A). For the quantification of Aβ, 0.5 mL of homogenate was centrifuged as described earlier. The pellet was delipidated with chloroform/methanol (2:1) and chloroform/methanol/water (1:2:0.8),[16] and the residue was extracted with 70% formic acid. An aliquot of the extract was then dried using a Speed Vac (Savant Instruments, Farmingdale, NY), solubilized with SDS sample buffer containing 4 *M* urea, and subjected to western blotting. Proteins separated on a 16.5% Tris-tricine gel were electrotransferred onto a nitrocellulose membrane. The membrane was then immersed in boiling phosphate-buffered saline to enhance the sensitivity[16] and probed with BA27 or BC05. Monomers of Aβ40/42 migrating at about 4 kd on the blots were quantified with an LAS-1000 Plus luminescent image analyzer using defined amounts of authentic Aβ40 or Aβ42 (Bachem, Bubendorf, Switzerland) as a standard (see figure 1B).

Statistical analysis. Statistical analyses were performed using Microsoft Excel 2001 (Microsoft, Redmond, WA) for linear regression analysis, StatView 5.0 for Kruskal–Wallis test, and JMP (SAS Institute, Cary, NC) for linear contrast. Trends for continuous variables were evaluated using analysis of variance with a linear contrast.

Results. Sarkosyl-insoluble tau was quantified as a relative score of Sarkosyl-insoluble tau (see Methods). The current protocol used here takes into account both PHF-tau at 68 kd and the tau-immunoreactive smear (see figure 1A). Thus, even smear-predominant samples, which were frequently encountered, can be quantified and compared. Regarding Aβ, only monomers were quantified as no authentic Aβ dimers are now available (see figure 1B). In cases with stage O for SPs, Aβ40 ranged from 0.3 to 3.6 pmol/g of wet wt and Aβ42 from 0.29 to 8.3 pmol/g of wet wt (see table). Among them, the levels of Aβ40 were mostly <1.5 pmol/g of wet wt, and those of Aβ42 were mostly <3 pmol/g of wet wt. These may be regarded as normal (monomer) levels for Aβ40/42. The maximum levels for Aβ42 in the entorhinal cortex were about 10^4 pmol/g of wet wt. These values are consistent with data by ELISA.[9,16]

Figure 2 shows the levels of insoluble tau and Aβ42 as a function of age. A possible longitudinal temporal profile

Table *Subjects used in this study*

No.	Age, y	Sex	PMI, h:min	Braak	SP	Aβ40	Aβ42	Insoluble tau	CDR	Aβ11–28	AT8
1	70	M	10:33	1	O	1.1	1.8	12.5	1	–	–
2	81	M	5:34	1	O	1.4	8.3	38.8	NA	–	–
3	86	M	2:00	1	O	0.96	1.6	150	0	–	+
4	78	M	6:45	1	A	0.66	2.3	22.9	NA	–	±
5	72	F	4:34	1	A	1.1	0.91	315	0	–	+–++
6	73	M	1:56	1	A	0.96	1.3	28.8	0	–	±
7	66	M	1:32	1	O	0.93	2	17.0	NA	–	–
8	69	M	2:00	1	O	1.1	0.48	97.1	0	–	±
9	68	M	7:33	1	O	0.96	0.29	31.4	0	–	–
10	68	M	4:15	1	O	2.5	1	309	0	–	+
11	74	F	15:15	1	O	1.6	2.2	97.9	1	–	±
12	81	M	2:14	1	O	1.3	0.52	111	0	–	+
13	78	F	7:15	1	A	0.79	67	385	0.5	+	+–++
14	77	F	9:27	1	A	2.8	1,600	74.3	0	+	±
15	77	M	9:32	1	A	1.3	49	756	0.5	±	–
16	78	F	18:14	1	A	1.5	248	58.9	0	±	–
17	63	F	6:00	1	A	1.1	1,300	34.1	1	+	–
18	53	M	9:01	1	B	1.85	1,830	22.4	NA	±	±
19	75	F	10:43	1	B	6.88	2,540	79.8	0	+–++	++
20	93	M	20:49	1	C	176	6,360	193	0.5	++	+
21	78	M	10:03	2	O	1.1	0.82	144	0	–	+–++
22	82	M	14:05	2	O	1.1	2.4	41.7	0.5	–	–
23	75	M	17:13	2	A	5.7	2,100	229	0	±	++
24	88	M	19:33	2	O	0.3	2.6	321	0	–	–
25	88	F	26:15	2	O/A	4.4	4.1	195	3	–	+
26	76	F	3:55	2	A	4.8	350	348	0.5	–	+
27	88	F	8:52	2	A	0.88	39	591	1	–	+++
28	77	M	2:47	2	A	0.73	16	28.9	0	–	+
29	73	F	3:32	2	B	3	2,900	207	0.5	+	+
30	81	M	6:15	2	B	16.2	3,580	273	0	++	+
31	78	F	10:24	2	B	1.19	3.2	475	0.5	–	++–+++
32	86	M	13:18	2	C	50.1	4,970	300	0	+++	+++
33	74	F	29:08	2	O	3.610	7.43	283	0	–	++
34	62	M	12:50	2	B	697	5,280	386	3	NE	++
35	76	M	6:30	2	C	157	4,050	178	0	+	+
36	87	F	24:28	3	B	9.4	4,000	47.1	NA	+	++
37	82	M	2:20	3	B	3,000	4,500	153	0	+	++
38	84	F	1:23	3	O	1.35	3.3	474	3	–	+
39	77	M	31:30	3	O	3.67	69	564	0	–	+–++
40	79	F	21:52	3	A	1.87	31.1	321	0	–	+++
41	91	F	1:27	3	A	7.9	981	570	0	+	++
42	87	F	4:21	3	C	57.7	3,720	530	0	++	+++
43	91	F	16:49	3	O	1.43	6.13	516	1	–	+++
44	81	F	8:02	3	A	15.1	125	211	0	NE	+–++
45	86	M	9:16	3	B	344	2,850	97.7	NA	++	+++
46	82	F	10:32	3	C	632	6,800	422	0.5	++	++
47	83	F	16:13	3.5	B	22	3,400	531	0	++	+++
48	89	M	7:10	4	B	23	3,400	707	1	++	+–++
49	92	F	4:35	4	C	459	6,600	435	2	++	++
50	85	F	14:20	4.5	C	1,190	11,700	439	2	++	+

Aβ40/42 is expressed in pmol/g of wet wt. The values of 3.5 and 4.5 for Braak NFT stage mean intermediate between stages III and IV and IV and V.

PMI = postmortem interval; Braak = Braak neurofibrillary tangle (NFT) stage: 1 (I), 2 (II), 3 (III), 4 (IV), 5 (V), and 6 (VI); SP = Braak senile plaque (SP) stage: O, A, B, and C (O stage indicates no SP, and O/A means intermediate between stages O and A); Aβ = amyloid β-protein; CDR = Clinical Dementia Rating Scale. Immunocytochemical scores for NFTs and SPs in the entorhinal cortex: (–) = none; (±) = scanty; (+) = some; (++) = moderate; (+++) = severe.

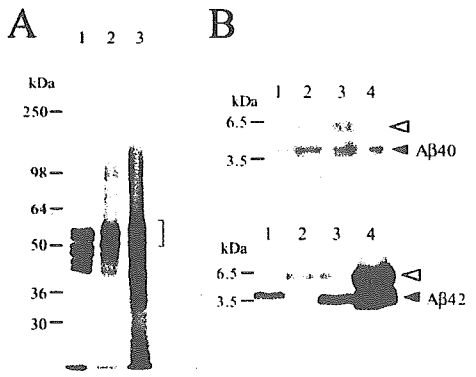

Figure 1. Western blots of insoluble fractions for the quantification of tau and amyloid β-protein (Aβ). (A) The defined amount of recombinant tau (six isoforms) was loaded in lane 1 (score, 100), Sarkosyl-insoluble fraction from Case 12 in lane 2 (111), and that from Case 40 in lane 3 (3,201). Paired helical filament–tau is indicated. (B) Authentic Aβ40 (10 pg) was loaded in lane 1, the insoluble fraction (corresponding to 7.5 mg of brain) from Case 15 in lane 2 (1.3 pmol/g), that from Case16 in lane 3 (1.5 pmol/g), and that from Case 4 in lane 4 (1.1 pmol/g; upper panel). Authentic Aβ42 (50 pg) was loaded in lane 1, the insoluble fraction (corresponding to 0.125 mg of brain) from Case 15 in lane 2 (49 pmol/g), that from Case 16 in lane 3 (248 pmol/g), that from Case 17 in lane 4 (1300 pmol/g). Filled arrowheads = Aβ40/42 monomers; open arrowheads = Aβ40/42 dimers.

can be reconstituted from these cross-sectional data. Although the number of younger cases (age <70 years) is relatively small, there is a strong tendency for a steep rise in the levels of tau starting at about age 75. Half of the 75-year-old and older subjects definitely exhibited abnormal levels of Aβ42 (>10 pmol/g of wet wt). The apparent steep rise in levels of Aβ42 is very similar to that reported for the prefrontal area (Brodmann areas 9 to 11)[16] but may be late (>10 years) compared with the neocortex.[16] According to the amyloid cascade hypothesis, this would suggest that acute deposition of Aβ42 in the entorhinal cortex at about age 75 promptly initiates NFT formation.

An increase in the levels of insoluble tau between Braak NFT stages I and II appeared not to continue between stages II and III (figure 3A; $p = 0.0024$, linear contrast), and no trend was observed between the levels of insoluble tau and Braak SP stages O and A to C (see figure 3B; $p > 0.05$, Kruskal–Wallis test). The levels of Aβ42 appeared to increase between Braak NFT stages I and II but did not show any further increase at stage III (see figure 3C; $p = 0.018$, linear contrast), whereas the levels of Aβ40 continued to increase from Braak NFT stages I to III (see figure 3D; $p = 0.001$, linear contrast). This situation resembles the prefrontal area.[16] It is possible that the accumulation of Aβ42 reaches a plateau early on, while Aβ40 does not. In sharp contrast to insoluble tau, Aβ42 accumulation definitely increases from Braak SP stages O and A to C (see figure 3E; $p < 0.001$, linear contrast). This indicates that the levels of insoluble tau in the entorhinal cortex do not increase from Braak NFT stages II to III, whereas the levels of Aβ42 increase from SP stages O and A to C. Therefore, the Braak NFT stage indicates the spread of NFT, as originally defined, but not the levels of insoluble tau, whereas the Braak SP stage is well correlated with levels of Aβ42 in the entorhinal cortex.

As expected, there was no correlation between the levels of insoluble tau and Aβ42 (figure 4; n = 50, $R^2 = 0.061$, $p > 0.05$) in the entorhinal cortex. Obviously, even if Aβ does not accumulate to significant extents, insoluble tau can accumulate to substantial extents in a number of specimens. Thus, the biochemical quantification confirms repeatedly reported observations showing that NFTs emerge in the entorhinal cortex without preceding SPs in the general population.[17]

Discussion. When scores for insoluble tau are compared with AT8 immunostains and values for Aβ42 with Aβ immunostains, there is generally a good correlation between biochemical and neuropathological measures (see table). In several cases, there are some discrepancies between the level of insoluble tau and AT8 score. These discrepancies could be generated because the epitope for AT8 is lost as intracellular NFTs evolve and are gradually converted to extracellular NFTs. Although we attempted to exclude subjects exhibiting argyrophilic and tau-immunopositive grains, some entorhinal cortices may have contained more grains (see table). The abundance of grains, which consists mainly of four-repeat tau, could have caused a significant devi-

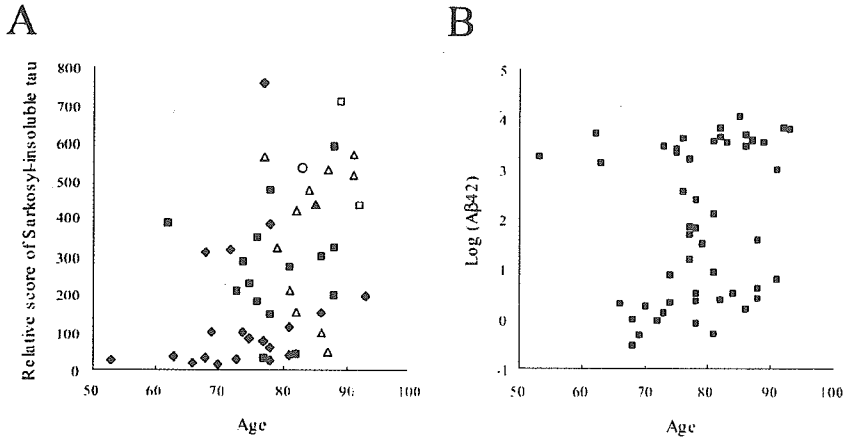

Figure 2. Accumulations of tau (A) and amyloid β-protein (Aβ) (B) in the entorhinal cortex as a function of age. (A) The levels of (Sarkosyl-)insoluble tau vs age. (B) log (Aβ42 [pmol/g]) vs age. Each mark represents one case. In A, diamonds = Braak neurofibrillary tangle stage I; filled squares = stage II; open triangles = stage III; open circles = stage 3.5 (defined as an intermediate between stages III and IV); open squares = stage IV; filled triangles = stage 4.5 (defined as an intermediate between stages IV and V).

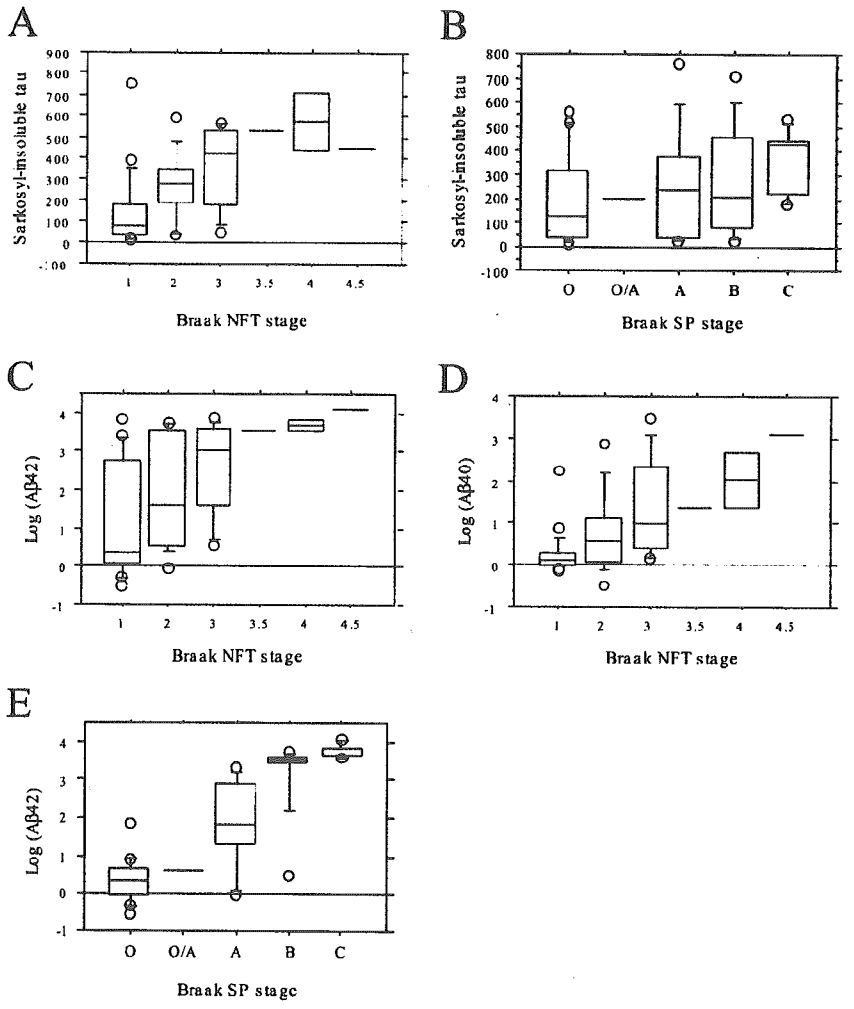

Figure 3. The levels of insoluble tau and amyloid β-protein (Aβ) 40/42 vs Braak stage for neurofibrillary tangles (NFTs) and senile plaques (SPs) (box-and-whisker plot). (A) Levels of insoluble tau vs Braak NFT stages. (B) Levels of insoluble tau vs Braak SP stage. (C) Aβ42 accumulation vs Braak NFT stage. (D) Aβ40 accumulation vs Braak NFT stage. (E) Aβ42 accumulation vs Braak SP stage. Circles indicate cases outside the 10th or 90th percentile in A to E.

ation in the insoluble tau score. However, even when the subjects with high burden of grains were removed, the same tendencies described above were observed (data not shown).

Only Aβ monomers were focused on here because authentic dimeric forms were unavailable. However, our previous data have shown that the levels of Aβ dimers are proportional to those of monomers.[16] Thus, the more abundant Aβ monomers are, the more abundantly dimers exist, although the absolute levels of the latter are unknown.

As the insoluble tau detected with pool-2 probably represents the total NFTs, both newly formed and aged NFTs, the latter of which are composed of processed tau,[13] the results indicate that the deposition of Aβ42 monomers (and so Aβ42 dimers) and NFT formation are not correlative and thus may occur independently in the entorhinal cortex. High values of Aβ42 did not significantly alter the accumulation levels of insoluble tau (see figure 4). In addition, the abundance of Aβ42 had no distinct effects on tau-immunoreactive bands and smears on the blots, when probed with iD387 or several phosphorylation-dependent antibodies (data not shown).

It is well known that the normal aged population

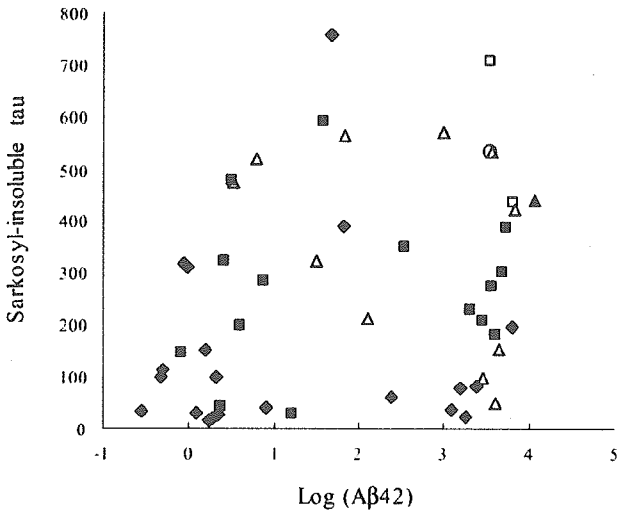

Figure 4. Amyloid β-protein (Aβ) 42 load and accumulation of insoluble tau. Each mark represents one case: diamonds = Braak stage I; filled squares = stage II; open triangles = stage III; open circles = stage 3.5; open squares = stage IV; filled triangles = stage 4.5.

always includes a certain proportion of preclinical AD cases (including MCI), which presents a serious problem in the interpretation of the data on the "normal" population. On the other hand, a great number of consecutive autopsy cases performed by Braak and Braak clearly indicate a continuous spectrum of the AD-related pathologies (NFTs and SPs) evolving during aging.[6,17] This suggests that very similar mechanisms are at work during aging, continuously bringing Braak stage I to VI. Of course, the presence of such AD-related pathologies does not necessarily mean clinical AD. However, a large fraction of these subjects with higher degrees of the pathologies seem to have clinical dementia.[6,17] Thus, it is reasonable to postulate that normal aging and AD are rather continuous from a pathologic point of view and that the presence of more than moderate pathologies is often associated with clinical dementia and with AD.

The current findings on the general aged population apparently contradict the widely accepted amyloid cascade hypothesis. It seems to be valid in the neocortex of patients with Down syndrome[18] and supported by recent experiments using transgenic mice. Breeding of APP- (β-amyloid precursor protein) transgenic mice (Tg2576) with P301L mice, which form NFTs exclusively in the brainstem and spinal cord, caused extensive NFT formation in the cortex,[19] never observed in the parental mice. In addition, injection of Aβ42 fibrils at the projection sites can accelerate NFT formation in the amygdaloid complex of P301L transgenic mice,[20] suggesting Aβ42 fibril-mediated retrograde degeneration.

In the entorhinal cortex, NFT formation appears to start from layer II stellate neurons, followed by layer IV neurons. One may argue that the axon terminals in the molecular layer of the dentate gyrus are first affected by Aβ42 accumulation, and the layer II stellate neurons degenerate in a retrograde manner. The histologic specimens barely exhibited SPs in the molecular layer at the same cut plane (anterior hippocampus). Thus, it is unlikely that retrograde degeneration results in NFT formation in layer II neurons of the entorhinal cortex.

A straightforward explanation for the current results is that the amyloid cascade hypothesis is valid in the neocortex but not in the hippocampus or the entorhinal cortex. This cannot explain accelerated alterations in both regions of the brain affected by familial AD. In fact, one report[21] documented the pathology of a subject having *PS1* mutation but presenting with no cognitive decline. This subject showed abundant Aβ42-positive SPs in the entorhinal cortex (and other areas) but virtually no NFTs, which is consistent with the amyloid cascade hypothesis. Thus, one possibility would be that there are two pathways for NFT formation in the entorhinal cortex, Aβ42-mediated and Aβ42-independent NFT formation, with the former tending to develop AD. Another possibility would be that an additional effect(s) of mutant APP and presenilin 1/2, besides increased production of Aβ42, leads to the premature NFT formation and degeneration in the hippocampus and entorhinal cortex. Increased intracellular Aβ42 accumulation[22,23] caused by mutant APP or presenilin 1/2 could have a significant role for enhanced neuronal degeneration in the hippocampus and entorhinal cortex in familial AD.

Acknowledgment

The authors thank Dr. H. Mori for providing pool-2 polyclonal antibodies and Dr. Y. Ito for help with statistical analysis.

References

1. Amaral DG, Insausti R. Hippocampal formation. In: Paxinos G, ed. The human nervous system. San Diego: Academic Press, 1990:711–755.
2. Sewards TV, Sewards MA. Input and output stations of the entorhinal cortex: superficial vs. deep layers or lateral vs. medial divisions? Brain Res Rev 2003;42:243–251.
3. Braak H, Braak E. Neuropathological stageing of Alzheimer-related changes. Acta Neuropathol (Berl) 1991;82:239–259.
4. Riley KP, Snowdon DA, Markesbery WR. Alzheimer's neurofibrillary pathology and the spectrum of cognitive function: findings from the Nun Study. Ann Neurol 2002;51:567–577.
5. Gold G, Bouras C, Kovari E, et al. Clinical validity of Braak neuropathological staging in the oldest-old. Acta Neuropathol (Berl) 2000;99: 579–582.
6. Duyckaerts C, Hauw JJ. Prevalence, incidence and duration of Braak's stages in the general population: can we know? Neurobiol Aging 1997; 18:362–369.
7. Kordower JH, Chu Y, Stebbins GT, et al. Loss and atrophy of layer II entorhinal cortex neurons in elderly people with mild cognitive impairment. Ann Neurol 2001;49:202–213.
8. Price JL, Morris JC. Tangles and plaques in nondemented aging and "preclinical" Alzheimer's disease. Ann Neurol 1999;45:358–368.
9. Funato H, Yoshimura M, Kusui K, et al. Quantitation of amyloid β-protein (Aβ) in the cortex during aging and in Alzheimer's disease. Am J Pathol 1998;152:1633–1640.
10. Gearing M, Mirra SS, Hedreen JC, et al. The Consortium to Establish a Registry for Alzheimer's Disease (CERAD). Part X. Neuropathology confirmation of the clinical diagnosis of Alzheimer's disease. Neurology 1995;45:461–466.
11. Shinkai Y, Yoshimura M, Ito Y, et al. Amyloid β-proteins (Aβ)1–40 and 1–42(43) in the soluble fraction of extra- and intracranial blood vessels. Ann Neurol 1995;38:421–428.
12. Endoh R, Ogawara M, Iwatsubo T, Nakano I, Mori H. Lack of the carboxyl terminal sequence of tau in ghost tangles of Alzheimer's disease. Brain Res 1993;601:164–172.
13. Watanabe A, Takio K, Ihara Y. Deamidation and isoaspartate formation in smeared tau in paired helical filaments. Unusual properties of the microtubule-binding domain of tau. J Biol Chem 1999;274:7368–7378.
14. Miyasaka T, Morishima-Kawashima M, Ravid R, et al. Molecular analysis of mutant and wild-type tau deposited in the brain affected by the FTDP-17 R406W mutation. Am J Pathol 2001;158:373–379.
15. Morishima-Kawashima M, Hasegawa M, Takio K, et al. Proline-directed and non-proline-directed phosphorylation of PHF-tau. J Biol Chem 1995;270:823–829.
16. Morishima-Kawashima M, Oshima N, Ogata H, et al. Effect of apolipoprotein E allele ε4 on the initial phase of amyloid β-protein accumulation in the human brain. Am J Pathol 2000;157:2093–2099.
17. Braak H, Braak E. Frequency of stages of Alzheimer-related lesions in different age categories. Neurobiol Aging 1997;18:351–357.
18. Mann DM. Cerebral amyloidosis, ageing and Alzheimer's disease: a contribution from studies on Down's syndrome. Neurobiol Aging 1989; 10:397–399.
19. Lewis J, Dickson DW, Lin WL, et al. Enhanced neurofibrillary degeneration in transgenic mice expressing mutant tau and APP. Science 2001; 293:1487–1491.
20. Gotz J, Chen F, van Dorpe J, Nitsch RM. Formation of neurofibrillary tangles in P301l tau transgenic mice induced by Aβ 42 fibrils. Science 2001;293:1491–1495.
21. Lippa CF, Nee LE, Mori H, St George-Hyslop P. Aβ-42 deposition precedes other changes in PS-1 Alzheimer's disease. Lancet 1998;352: 1117–1118.
22. Qi Y, Morishima-Kawashima M, Sato T, Mitsumori R, Ihara Y. Distinct mechanisms by mutant presenilin 1 and 2 leading to increased intracellular levels of amyloid β-protein 42 in Chinese hamster ovary cells. Biochemistry 2003;42:1042–1052.
23. Oddo S, Caccamo A, Shepherd JD, et al. Triple-transgenic model of Alzheimer's disease with plaques and tangles: intracellular Aβ and synaptic dysfunction. Neuron 2003;39:409–421.

Am. J. Hum. Genet. 77:280–296, 2005

An Autosomal Dominant Cerebellar Ataxia Linked to Chromosome 16q22.1 Is Associated with a Single-Nucleotide Substitution in the 5′ Untranslated Region of the Gene Encoding a Protein with Spectrin Repeat and Rho Guanine-Nucleotide Exchange-Factor Domains

Kinya Ishikawa,[1,*] Shuta Toru,[1,*] Taiji Tsunemi,[1] Mingshun Li,[1] Kazuhiro Kobayashi,[8] Takanori Yokota,[1] Takeshi Amino,[1] Kiyoshi Owada,[1] Hiroto Fujigasaki,[1] Masaki Sakamoto,[1] Hiroyuki Tomimitsu,[1] Minoru Takashima,[1] Jiro Kumagai,[2] Yoshihiro Noguchi,[3] Yoshiyuki Kawashima,[3] Norio Ohkoshi,[9] Gen Ishida,[10] Manabu Gomyoda,[11] Mari Yoshida,[12] Yoshio Hashizume,[12] Yuko Saito,[5] Shigeo Murayama,[5] Hiroshi Yamanouchi,[6] Toshio Mizutani,[7] Ikuko Kondo,[13] Tatsushi Toda,[8] and Hidehiro Mizusawa[1,4]

Departments of [1]Neurology and Neurological Science, [2]Pathology, and [3]Audiovestibular Science, Graduate School, and [4]The 21st Century Center of Excellence Program on Brain Integration and Its Disorders, Tokyo Medical and Dental University, [5]Department of Neuropathology, Tokyo Metropolitan Institute of Gerontology, [6]Department of Neurology, Tokyo Metropolitan Geriatric Hospital, and [7]Department of Pathology, Tokyo Metropolitan Neurological Hospital, Tokyo; [8]Division of Functional Genomics, Department of Post-Genomics and Diseases, Course of Advanced Medicine, Osaka University Graduate School of Medicine, Osaka, Japan; [9]Department of Neurology, Institute of Clinical Medicine, University of Tsukuba, Tsukuba, Japan; Departments of [10]Neurology and [11]Clinical Laboratory, National Matsue Hospital, Matsue, Japan; [12]Department of Neuropathology, Institute of Medical Science of Aging, Aichi Medical University, Aichi, Japan; and [13]Department of Medical Genetics, Ehime University School of Medicine, Ehime, Japan

Autosomal dominant cerebellar ataxia (ADCA) is a group of heterogeneous neurodegenerative disorders. By positional cloning, we have identified the gene strongly associated with a form of degenerative ataxia (chromosome 16q22.1–linked ADCA) that clinically shows progressive pure cerebellar ataxia. Detailed examination by use of audiogram suggested that sensorineural hearing impairment may be associated with ataxia in our families. After restricting the candidate region in chromosome 16q22.1 by haplotype analysis, we found that all patients from 52 unrelated Japanese families harbor a heterozygous C→T single-nucleotide substitution, 16 nt upstream of the putative translation initiation site of the gene for a hypothetical protein DKFZP434I216, which we have called "puratrophin-1" (Purkinje cell atrophy associated protein-1). The full-length *puratrophin-1* mRNA had an open reading frame of 3,576 nt, predicted to contain important domains, including the spectrin repeat and the guanine-nucleotide exchange factor (GEF) for Rho GTPases, followed by the Dbl-homologous domain, which indicates the role of puratrophin-1 in intracellular signaling and actin dynamics at the Golgi apparatus. Puratrophin-1—normally expressed in a wide range of cells, including epithelial hair cells in the cochlea—was aggregated in Purkinje cells of the chromosome 16q22.1–linked ADCA brains. Consistent with the protein prediction data of puratrophin-1, the Golgi-apparatus membrane protein and spectrin also formed aggregates in Purkinje cells. The present study highlights the importance of the 5′ untranslated region (UTR) in identification of genes of human disease, suggests that a single-nucleotide substitution in the 5′ UTR could be associated with protein aggregation, and indicates that the GEF protein is associated with cerebellar degeneration in humans.

Introduction

Autosomal dominant cerebellar ataxia (ADCA) is a clinical entity of heterogeneous neurodegenerative diseases that show dominantly inherited, progressive cerebellar ataxia that can be variably associated with other neurological and systemic features (Harding 1982). Circumscribed groups of neurons in the cerebellum, brainstem, basal ganglia, or spinal cord are selectively involved in different combinations and to varying extents among diseases (Graham and Lantos 2002). ADCA is now classified by the responsible mutations or gene loci. To date, 24 subtypes have been identified: spinocerebellar ataxia type (SCA) 1, 2, 3 (or, Machado-Joseph disease [MJD]), 4–8, 10–19/22, 21, 23, 25, 26; dentatorubral and pallidoluysian atrophy (DRPLA); and ADCA with mutation in fibroblast growth factor (FGF) 14 (Stevanin et

Received March 15, 2005; accepted for publication June 3, 2005; electronically published July 6, 2005.

Address for correspondence and reprints: Dr. Hidehiro Mizusawa, Professor and Chairman, Department of Neurology and Neurological Science, Graduate School, Tokyo Medical and Dental University, 1-5-45 Yushima, Bunkyo-ku 113-8519, Tokyo, Japan. E-mail: h-mizusawa.nuro@tmd.ac.jp

* These two authors contributed equally to this work.

0002-9297/2005/7702-0010$15.00

al. 2000, 2004; Margolis 2002; van Swieten et al. 2003; Yu et al. 2005). Among these, mutations in SCA1, SCA2, SCA3/MJD, SCA6, SCA7, SCA17, and DRPLA have been identified as the expansion of a trinucleotide (CAG) repeat that encodes the polyglutamine tract, uniformly causing aggregation of polyglutamine-containing causative protein (Ross and Poirier 2004). Expansion of noncoding trinucleotide (CAG or CTG) or pentanucleotide (ATTCT) repeats are involved in SCA8, SCA10, and SCA12 (Holmes et al. 1999; Koob et al. 1999; Matsuura et al. 2000). Very few families are affected by missense mutations in the protein kinase Cγ (PKCγ) (SCA14 [see Chen et al. 2003]) and *FGF14* genes (ADCA with *FGF14* mutation [see van Swieten et al. 2003]). However, genes or even their loci remain unidentified for >20%–40% of families with ADCA (Sasaki et al. 2003).

We had previously mapped mutations in six Japanese families with ADCA to a 10-cM interval in human chromosome 16q13.1-q22.1, identifying 16q-linked ADCA type III, or spinocerebellar ataxia 4 (SCA4 [MIM 600223]) (Ishikawa et al. 2000). Clinically, our families show cerebellar ataxia without obvious evidence of extracerebellar neurological dysfunction (i.e., "pure cerebellar ataxia," or "ADCA type III") (Harding 1982; Ishikawa et al. 2000). The average age at onset of ataxia was >55 years (Ishikawa et al. 1997), which suggests that this disease shows the oldest age at onset among ADCA types with assigned loci. Another important clinical feature of this disease is that a substantial number of patients show progressive sensorineural hearing impairment (Owada et al., in press). Since the hearing impairment can be very mild and of later onset, presence of hearing impairment can be easily overlooked. However, this finding may indicate that the mutated gene could cause hearing impairment as well as ataxia. In this sense, it would be more appropriate to use the term "chromosome 16q22.1–linked ADCA" instead of "ADCA type III" to describe our families. Neuropathological examination showed peculiar degeneration of Purkinje cells that was not described in other degenerative ataxias (Owada et al., in press). Many Purkinje cells undergo shrinkage and are surrounded by amorphous materials composed of Purkinje-cell somato-dendritic sprouts and an increased number of presynaptic terminals. These findings may indicate that certain proteins involved in the cytoskeleton of Purkinje cells are disturbed in chromosome 16q22.1–linked ADCA.

Chromosome 16q22.1–linked ADCA has been assigned to the same locus as another ADCA, SCA4 (Flanigan et al. 1996; Hellenbroich et al. 2003). Although SCA4 and chromosome 16q22.1–linked ADCA may be allelic, SCA4 is clinically distinct from chromosome 16q22.1–linked ADCA, because SCA4 shows prominent sensory axonal neuropathy and pyramidal tract signs, with an age at onset earlier than that of chromosome 16q22.1–linked ADCA (Flanigan et al. 1996; Hellenbroich et al. 2003). Several groups, including ours, have refined the loci of SCA4/chromosome 16q22.1–linked ADCA and have, so far, excluded repeat expansions as mutations (Hellenbroich et al. 2003; Li et al. 2003; Hirano et al. 2004). The minimum candidate region of SCA4 and chromosome 16q22.1–linked ADCA is set at the region between markers *D16S3031* and *D16S3095*. A strong founder effect has been observed for chromosome 16q22.1–linked ADCA (Li et al. 2003), which indicates the need to recruit a large number of families to narrow the critical region.

To discover the causative gene of chromosome 16q22.1–linked ADCA, we embarked on a positional cloning study by recruiting 52 families from diverse regions of Japan. Here, we describe the identification of a strong association between a single-nucleotide change and chromosome 16q22.1–linked ADCA and show the consequence of this genetic change on mRNA and protein levels. The data presented here also suggest that a single-nucleotide change in the 5′ UTR could be associated with aggregation of the gene product.

Patients, Material, and Methods

Recruitment of Families with Chromosome 16q22.1–Linked ADCA

We attempted to include families clinically diagnosed with late-onset ADCA type III from a wide region of Japan. Fifty-two families, including 109 affected individuals and 48 at-risk individuals, were ultimately recruited. These families originated from seven of eight districts of Japan (Hokkaido, Tohoku, Kanto, Chu-bu, Kinki, Chu-goku, and Kyu-shu), which indicates that their origins are widespread. Clinical features of these patients were consistent with those of families described elsewhere (Ishikawa et al. 1997, 2000; Li et al. 2003).

Detailed neuro-otological examinations, including pure-tone audiometry, were performed on 13 families at the Departments of Neurology and Otolaryngology, Tokyo Medical and Dental University. Progressive hearing impairment was assessed when the pure-tone average calculated from thresholds at the frequencies of 0.5, 1, and 2 kHz was more severe than the mean +2 SD of age-matched normal Japanese population (Tsuiki et al. 2002). By that criterion, 6 (42.9%) of 14 families had a hearing impairment other than age-related hearing loss. When we used the recommendations for the description of genetic and audiological data composed by the GENDEAG study group (see The Hereditary Hearing Loss Homepage), all of the patients with the hearing impairment were confirmed to have bilateral sensorineural hearing loss of mild-to-moderate severity. The audiometric configurations of these patients include mid-fre-

quency U-shaped, flat, and high-frequency sloping. These data would suggest that the hearing impairment in our families is not a coincidence.

Preparation of DNA and RNA Samples

After informed consent was obtained, genomic DNA was extracted from peripheral-blood lymphocytes or lymphoblastoid cell lines by use of methods described elsewhere (Ishikawa et al. 1997). All families were excluded for SCA1, SCA2, SCA3/MJD, SCA6, SCA7, SCA8, SCA12, SCA14, SCA17, and DRPLA by testing mutations in the disease genes. For expression analysis on an RNA level, frozen cerebellar tissues of four brains affected with Alzheimer disease (AD) (age at death, range 65–85 years; duration of the disease, range 5–10 years) were used as controls. Clinically, these patients with AD showed a moderate-to-severe degree of dementia, as measured by the Clinical Dementia Rating (Hughes et al. 1982). Neuropathology in the cerebella of these patients showed only a few senile plaques without neuronal losses. For chromosome 16q22.1–linked ADCA, two patients were studied (ages at death, 74 and 78 years). Both control and 16q22.1-linked ADCA brains were obtained at autopsy, with the families' written consents approved by each institutional ethical committee. These brains were immediately frozen and stored at −80°C until use. Total RNA was extracted from frozen cerebellar tissues as described elsewhere (Ishikawa et al. 1999). Poly-A^+ RNA was selected from total RNA by NucleoTrap (Macherey-Nagel).

Restriction of Candidate Interval by Genotyping and Haplotype Analysis

Genotypes were determined for 23 informative markers, including five new markers we identified (*GGAA10, TTCC01, TA001, GA001,* and *AAT01* [GenBank accession numbers AB13610, AB13611, AB13612, AB197662, and AB13613, respectively]) (table 1). Standard PCR was performed in a final volume of 20 μl, containing 10 ng of genomic DNA, 3.4 pmol of each primer, 2.5 mM of dNTP, and 0.75 U of *Taq* polymerase (Takara). Thermal cycling was performed at 94°C for 5 min for initial denaturing, 30 cycles of denaturation (94°C for 30 s), annealing (55°C for 30 s), and extension (72°C for 30 s), followed by a final extension at 72°C for 5 min in an ABI GeneAmp PCR system 9700 (PE Applied Biosystems). The amplified product was separated in the Automated Laser Fluorescent DNA Sequencer II (Pharmacia Biotech), and genotypes were determined with Fragment Manager (Pharmacia Biotech) (Ishikawa et al. 1997). Allele frequencies in the general population were analyzed in 500 unrelated individuals without personal or family history of ataxia or other degenerative diseases.

Table 1

Microsatellite Markers and Primer Sequences

The table is available in its entirety in the online edition of *The American Journal of Human Genetics.*

Haplotypes of 16q22.1 markers were determined for 10 families (fig. 1) that were informative for determining the phase of alleles. The remaining 42 families were not sufficiently informative for determining the phase. Paucity of informative families was mainly due to the late age at onset of this disease. For these uninformative families, only combinations of genotypes were assessed, and the region of genotypes shared with the larger 10 families was compared.

Screening for Mutation in 21 Different Candidate Genes

Within the most critical interval, 21 genes or clusters of ESTs were retrieved from the Ensembl, UniGene, National Center for Biotechnology Information (NCBI), and Celera databases. Primers were designed to amplify individual exon and intron-exon boundaries for each gene, and genomic DNA was amplified by the aforementioned standard PCR protocol (primer sequences are available on request). Amplicons from controls and patients were first separated on 2% agarose gels, to determine by screening whether any aberrant bands were amplified from patient DNA samples. Residual solutions of PCR products were then purified with QIAquick PCR purification kit (Qiagen) and were directly sequenced using Applied Biosystems Model 377 or 3100 Automated Sequencer, as described elsewhere (Li et al. 2003). The mutation was analyzed by comparing sequenced data and annotated databases, with use of the software DNASIS (Hitachi). Genomic rearrangement was screened by Southern-blot analysis by use of cosmid clones for probe synthesis as described elsewhere (Kobayashi et al. 1998). In brief, cosmid clones, tandemly covering the chromosome 16q22.1–linked ADCA critical region, were generated by subcloning from the BAC contig (Li et al. 2003). Then, the radiolabeled (^{32}P) probe was generated from each cosmid clone. Genomic DNA extracted from lymphoblastoid cell lines of control individuals and patients with chromosome 16q22.1–linked ADCA was digested with a restriction enzyme and was subjected to Southern-blot analysis. To screen gene arrangement, analysis was performed with six different restriction enzymes (*Bam*HI, *Bgl*II, *Eco*RI, *Eco*RV, *Hind*III, and *Xba*I).

Twenty-one exons and 20 introns of the *puratrophin-1* gene, partially annotated as "*Q9H7K4,*" were sequenced entirely. The genomic region between the *puratrophin-1* gene and *SLC9A5* was also screened (fig. 2).

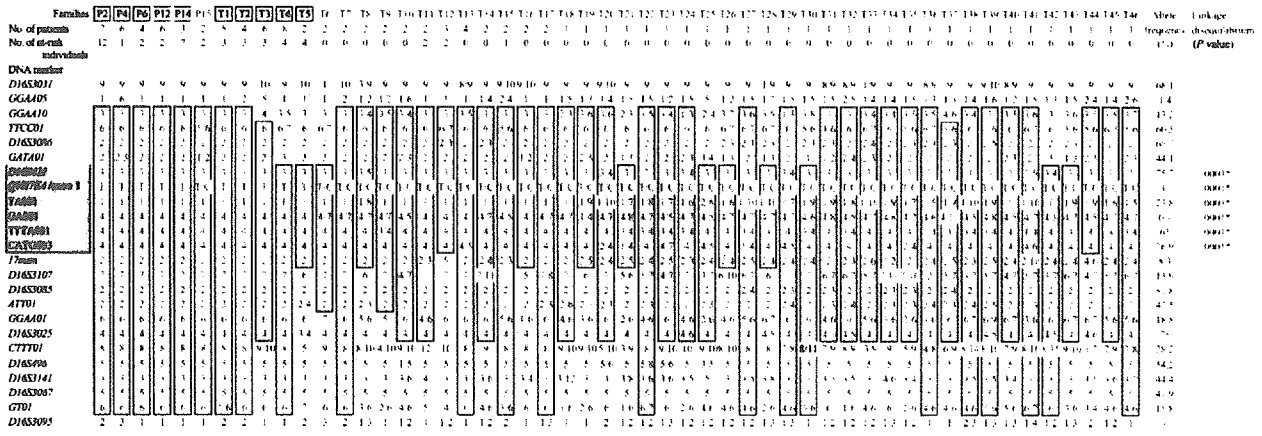

Figure 1 Haplotype analysis in the chromosome 16q22.1–linked ADCA critical locus. Ten families (P2, P4, P6, P12, P14, and T1–T5) large enough for haplotype analysis are indicated (*yellow boxes at top*). A founder haplotype "3-1-4-4-4" was seen in all patients for markers 16cen-*D16S421-TA001-GA001-TTTA001-CATG003*-16qter, between *GATA01* and *17msm*. Two alleles are shown (separated by a virgule [/]) for cases in which phase could not be determined. An asterisk (*) indicates that *P* values show significant linkage disequilibrium by Fisher's exact probability test. The specific C→T change in the *puratrophin-1* gene lies within the founder chromosomal region.

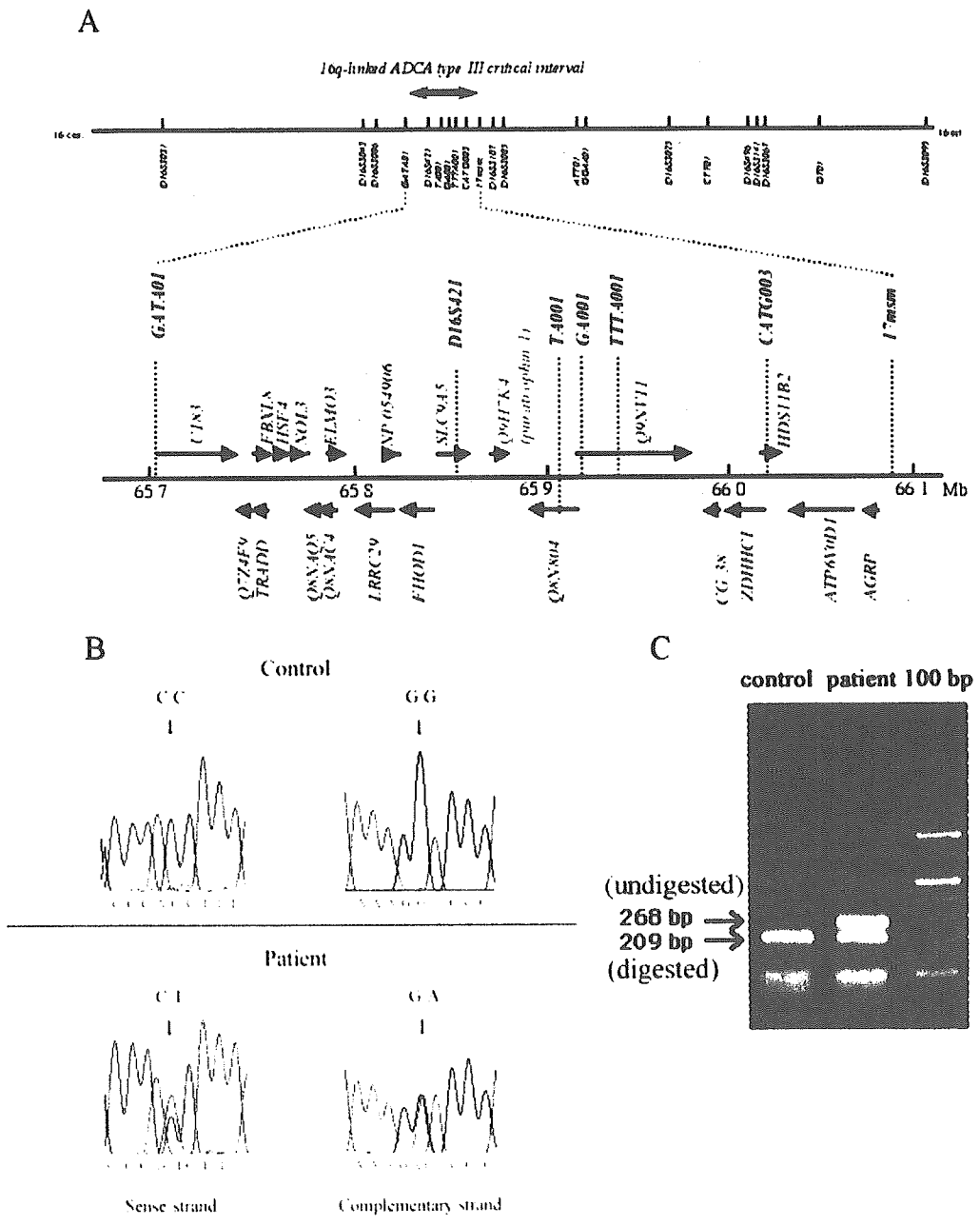

Figure 2 Positional cloning of the chromosome 16q22.1–linked ADCA gene. *A*, Genetic and physical maps of the interval in chromosome 16q22.1, showing microsatellite markers used to refine the interval. Twenty-one genes and their direction of transcription (Ensembl) are shown. *B*, Nucleotide sequences of exon 1 flanking the C→T single-nucleotide change in control and patient DNA samples. The patient harbors a heterozygous C→T substitution on the sense strand. *C*, RFLP by digestion with *Eco*NI. PCR was performed with primers UK1-E1F1 and UK1-E1R1. Whereas the normal allele produces digested fragments of 209, 92, and 59 bp, the C→T change in the mutant allele disrupts one *Eco*NI site, producing fragments of 268 and 92 bp.

The C→T change in the 5′ UTR was detected by amplifying genomic DNA with forward primer UK1-E1F1 (5′-CAGCGCGGTTCACACTGAGA-3′) and reverse primer UK1-E1R1 (5′-GGCCCTTTCTGACAGGACTGA-3′), which yielded a specific product of 360 bp. This amplicon harbors two *Eco*NI sites, one of which is destroyed by the C→T change.

Expression Analysis of Puratrophin-1 *mRNA by RT-PCR*

To characterize *puratrophin-1* mRNA in the human brain, poly-A$^+$RNA obtained from control human cerebellar tissues was reverse transcribed with SuperScript II (Stratagene), and the entire coding region was amplified with primers UKI-RT-025F (5′-TTCGCCTGCATTGCCCACTGAG-3′) and UK1-RT-005R (5′-CACACACATCAGAAAGGGTAGTCAAC-3′), which yielded a major product of 3,835 bp. To analyze alternative transcription, the PCR products were subcloned into pCR2.1-TOPO (Invitrogen), and 10 randomly selected clones from each brain mRNA (2 AD and 2 chromosome 16q22.1–linked ADCA cerebella) were sequenced and compared with partially annotated sequences (*Q9H7K4*, NCBI accession numbers BC054486 and AK024475). Rapid cloning of the 5′ and 3′ ends (5′- and 3′-RACE) was performed using Marathon-ready cDNA kit (Clontech [BD Biosciences]) as described elsewhere (Tsunemi et al. 2002). The entire 5′ UTR was amplified with primers UK1-RT-493F (5′-TGAGACAGTCTCAGTCAGGTCAC-3′) and UK1-RT-021R (5′-GTGGGCACACAGAAGCAGCACTGC-3′), was subcloned into pCR2.1-TOPO (Invitrogen), and was sequenced.

Expression of the *puratrophin-1* gene in various human tissues was studied by RT-PCR with use of primers UKI-RT-025F and UK1-RT-005R on human Multiple Tissue Panels I and II (Clontech [BD Bioscience]). Expression levels of *puratrophin-1* mRNA were compared among control and patient cerebellar cortices by RT-PCR with use of primers UK1-RT-BF001F (5′-TCACGGTTCCCCGCGGCTCG-3′) and UK1-RT-BF019R (5′-GGTTGCATGGCCCTGAGAGTCTGG-3′), which yielded PCR products of 291, 419, and 505 bp, depending on alternative transcription. To compare *puratrophin-1* mRNA levels more precisely, real-time RT-PCR analysis was performed on four control (individuals with AD) and two chromosome 16q22.1–linked ADCA cerebella by use of TaqMan technique (Applied Biosystems) on Applied Biosystems 7700 Sequence Detection System. PCR was performed for total *puratrophin-1* mRNAs (i.e., full-length and short-form mRNAs [GenBank accession numbers AB197663 and AB197664, respectively]; definitions of these two isoforms are described in the "Results" section) with primers total-taq-F (5′-TGGAGAGATGAGTGTCAAGACTTTG-3′) and total-taq-R (5′-AATGACTTGGGTCTGCCTTGG-3′). The short-form *puratrophin-1* mRNA was specifically assessed with primers short-taq-F (5′-ATGCCACCGACTGGAGATTT-3′) and short-taq-R (5′-GCTGCCCTGTAGCTCCTCAT-3′). The TaqMan probe for total *puratrophin-1* mRNA was 5′-FAM-CCAGATGCACGTTAAGGACCCAGGTC-TAMRA-3′, and that for short-form *puratrophin-1* mRNA was 5′-FAM-TCTCTGACCCTACTCAGGCTGAAGCCC-TAMRA-3′. The experiments were performed three times and were averaged. The level of *puratrophin-1* mRNA was assessed relative to the level of *G3PDH* mRNA amplified with primers supplied from the manufacturer (Applied Biosystems). Since the expression level of *G3PDH* mRNA was >1,000-fold higher than that of *puratrophin-1* mRNA, one control individual was chosen and the value of *puratrophin-1* mRNA:*G3PDH* mRNA ratio (designated "*puratrophin-1* mRNA/*G3PDH* mRNA index") was standardized as "1"; another three control individuals and two patients were compared relatively. The difference between the control and patient groups was statistically analyzed with the Mann-Whitney *U* test.

To see the effect of the C→T change in the 5′ UTR of *puratrophin-1* gene on expression in vitro, the partial 5′-UTR fragment containing the mutation site was amplified with forward primers UK1-UF10-F2 (5′-CCGGAATTCCAGGCCTGAATTGCAGTTC-3′) and UK1-UF10-R2 (5′-CCAGGCATCCCTGAAACT-3′) and was subcloned into the *Hind*III-*Nco*I sites of the luciferase assay vector, pGL3-Control Vector (Promega). The C→T mutation was then generated by site-directed mutagenesis (Stratagene). Three types of vectors (mock, empty pGL3-Control Vector; wild-type, pGL3 with normal *puratrophin-1* 5′ UTR with allele C; and mutant, pGL3 with mutant *puratrophin-1* 5′ UTR with allele T) were separately transfected with Renilla vector (Promega) into HEK293 cells to equalize the transfection efficiency. The transfection experiment was performed independently three times. Luciferase activity (F/R: fire-fly luciferase activity against Renilla activity) was assayed in accordance with the manufacturer's protocol and was statistically analyzed with the Mann-Whitney *U* test.

Generation of Rabbit Polyclonal Antibodies against Puratrophin-1

On the basis of the deduced amino acid sequence of "full-length" and "short-form" puratrophin-1, the secondary structure of each isoform was predicted, and five synthetic peptides were designed: polypeptide *FL01* (aa 1–13), N-MERPLENGDESPD-C; *FL02* (aa 421–432), N-MDKADELYDRVD-C; *FL03* (aa 570–583), N-EEGQRVLAELEQER-C; *FL04* (aa 991–1003), N-RFEIWFRRRKARD-C; and *SV01* (aa 13–26), N-REVWEGNGDAWRDE-C. The polypeptide FL01 lies at the amino terminus of the puratrophin-1 (fig. 3). Therefore, the

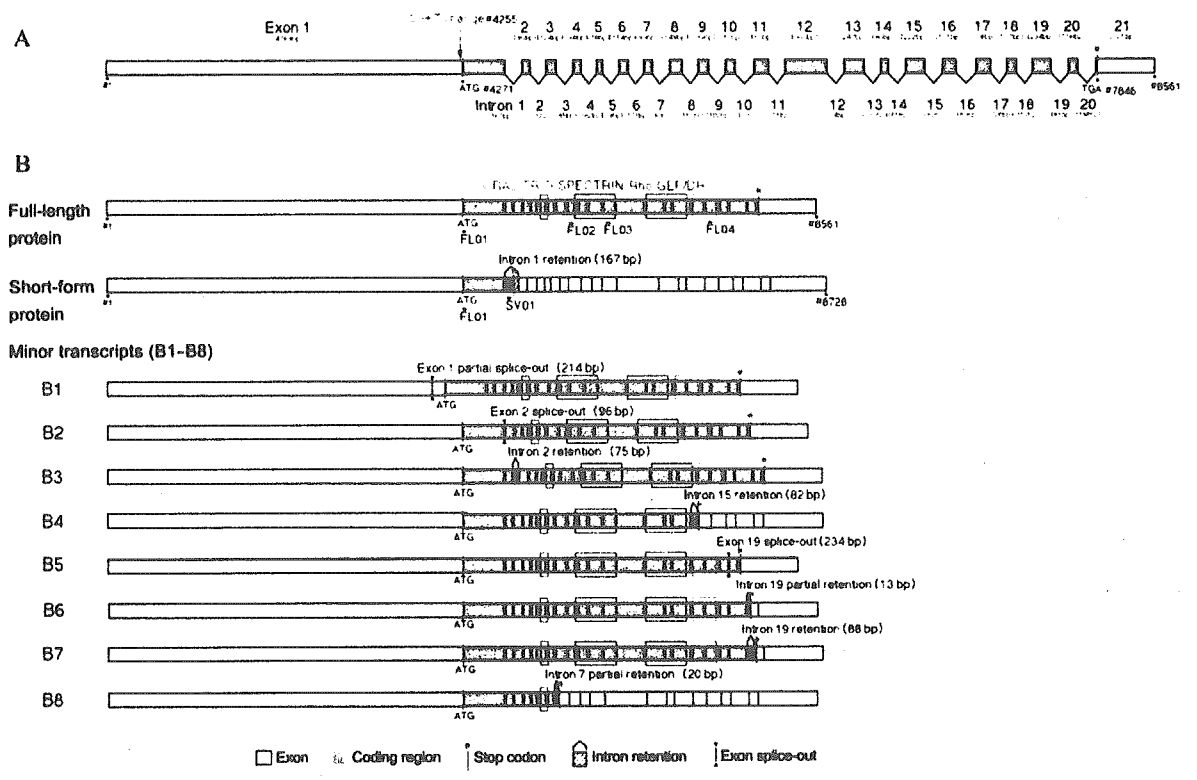

Figure 3 Genomic and mRNA structure of the *puratrophin-1* gene. *A*, Intron-exon structure of *puratrophin-1*. Exons are shown as vertical bars, and coding regions are shown in red. The C→T change at nt 4255 (or, 16 nt upstream of the translation initiation codon) is indicated. Nucleotide numbers (indicated by a number sign [#]) are counted from the 5′ end. *B*, *Puratrophin-1* mRNAs cloned from the human cerebellum. Major transcripts are full-length and short-form *puratrophin-1* mRNAs; minor transcripts (B1–B8) were also cloned. The CRL-TRIO, spectrin, Rho GEF/DH, and PH domains are indicated. Epitopes for five rabbit anti–puratrophin-1 antibodies (FL01–FL04 and SV01) are also mapped. Antibodies FL02, FL03, and FL04 are designed to specifically detect full-length puratrophin-1, the antibody SV01 specifically detects short-form puratrophin-1, and the antibody FL01 detects both full-length and short-form puratrophin-1.

antibody Prtrphn1-Ab FL01 would detect both full-length and short-form puratrophin-1. The polypeptides FL02, FL03, and FL04 are specific for the full-length puratrophin-1 (fig. 3). Notably, FL03 is at the spectrin repeat motif. The polypeptide SV01 lies at the carboxyl-terminus of the short-form puratrophin-1. Therefore, the antibody Prtrphn1-Ab SV01 would specifically recognize the short-form puratrophin-1. Each antigen was immunized into rabbit, and polyclonal antibodies were obtained as described elsewhere (Ishikawa et al. 1999).

The specificity of Prtrhn1-Abs was assessed by detection of recombinant puratrophin-1 protein. For this purpose, an antisense-strand primer was designed to encode hemagglutinin A (HA) in-frame at the carboxyl-terminus of the puratrophin-1. By PCR, full-length *puratrophin-1* cDNA with the HA-coding nucleotide sequence at its 3′ end was generated and was then cloned into pcDNA1 expression vector (Invitrogen). The puratrophin-1–HA fusion protein, transiently expressed in HEK293 cells, was first immunoprecipitated with Prtrhn1-Abs and then was detected with rat monoclonal anti-HA High Affinity antibody (3F10 [Roche Mannheim]) (fig. 4). The fusion protein immunoprecipitated with preimmune sera was not detected with anti-HA antibody.

Specificity of Prtrphn1-Abs on immunohistochemistry was assessed by immunoabsorption test. Solutions containing Prtrphn1-Ab and different concentrations of antigen (synthetic peptide) (0, 0.01, 0.1, and 1 mg/

The figure is available in its entirety in the online edition of *The American Journal of Human Genetics*.

Figure 4 Immunoprecipitation of puratrophin-1–HA fusion protein and immunoabsorption test with antiserum against puratrophin-1. The legend is available in its entirety in the online edition of *The American Journal of Human Genetics*.

liter) were made. Sections were incubated overnight with these solutions as other immunohistochemical staining. Prtrphn1-Abs were completely absorbed by peptides of higher concentrations (fig. 4).

Immunohistochemical Analyses of Puratrophin-1, Golgi-Apparatus Protein G58K, and Spectrin in Control Mouse, Human, and 16q22.1-Linked ADCA Tissues

Five polyclonal antibodies against puratrophin-1 (Prtrphn1-Ab types *FL01*, *FL02*, *FL03*, *FL04*, and *SV01*) were used for immunohistochemistry. Mouse monoclonal antibody against the microtubule-binding peripheral Golgi-apparatus membrane protein G58K (Sigma) and the mouse monoclonal antibody for α- and β-spectrin (MAB372 [Chemicon International]) were also used for immunohistochemistry.

Formalin-fixed paraffin-embedded tissue sections were prepared. Examined tissues were C57BL/6J wild-type mouse tissue, including cochlea (1 d postnatal), normal-control human tissues (testis, pancreas, prostate gland, lung, liver, heart, kidney, and brain from three individuals who died with nonneurological diseases), disease-control human brains (AD [n = 3], SCA6 [n = 2], multiple-system atrophy [MSA] [n = 3], and SCA3/MJD [n = 3]), and three brains with chromosome 16q22.1–linked ADCA. Immunohistochemistry was performed as described elsewhere (Ishikawa et al. 1999). In brief, sections were incubated overnight with Prtrphn1-Abs (diluted 1:200 with PBS), G58K (diluted 1:400), or MAB372 (diluted 1:200) at 4°C, after which the primary antibody was serially detected with avidin-biotinylated peroxidase complex method (Vector), was developed with 3,3′-diaminobenzidine (DAB), and was counterstained with hematoxylin.

Results

Restriction of the Critical Interval to <600 kb within Human Chromosome 16q22.1

Haplotype reconstruction of 10 informative families revealed that all affected individuals in these families were segregated with the haplotype 3-1-4-4-4 for markers *16cen-D16S421-TA001-GA001-TTTA001-CATG003-16qter* lying between *GATA01* and *17msm* (fig. 1). Genotypes of all affected individuals in the remaining 42 families that were not informative enough for haplotype reconstruction were also consistent with the common haplotype. Particularly, a dinucleotide (GA) repeat marker *GA001* showed strong linkage disequilibrium: the allele 4 of GA001 was seen in all affected individuals in all families with chromosome 16q22.1–linked ADCA, whereas that allele was seen very rarely (frequency 0.1%) in 1,000 control chromosomes (fig. 1). Whereas only one common haplotype was seen between *GATA01* and *17msm*, different alleles were seen for *GATA01* and other centromeric markers or for *17msm* and other telomeric markers (fig. 1). These results indicate that the gene for chromosome 16q22.1–linked ADCA is most likely to exist in the interval between *GATA01* and *17msm*. This region was within the previously refined intervals (Hellenbroich et al. 2003; Li et al. 2003) and was considered to be <600 kb in size in the database Ensembl.

Identification of a Single-Nucleotide Substitution in the 5′ UTR of the Gene Encoding Puratrophin-1 in the Critical Interval

Within the critical interval between *GATA01* and *17msm*, 21 different genes were identified (fig. 2*A*). We screened all 21 genes by direct sequencing of amplified genomic PCR products of all coding exons and flanking intronic sequences. Genomic Southern-blot analyses were also performed but did not detect any rearrangement (fig. 5).

We found that all patients with chromosome 16q22.1–linked ADCA harbored a heterozygous C→T single-nucleotide substitution at the position 16 nt upstream of the putative translation initiation codon of the gene *Q9H7K4*, encoding hypothetical protein DKFZP434I216 (NCBI accession number BC054486) (fig. 2*B*). All the at-risk individuals who had the founder haplotype between *GATA01* and *17msm* also harbored the C→T change. The ages of these individuals were below the maximum age at disease onset in their families, which indicates that they could be in presymptomatic stages. On the other hand, this C→T substitution was not seen in 500 healthy Japanese individuals (1,000 chromosomes), confirmed by *Eco*NI RFLP analysis (fig. 2*C*). All intronic sequences between the 21 exons and all the 8-kb sequences upstream of the *Q9H7K4* gene were also directly sequenced. Although there was a G→A SNP 44 nt upstream of the 3′ splice site of intron 9 of the *Q9H7K4* gene, the allele segregating with the disease was also seen in 75% of control chromosomes. As far as we examined, the C→T change at the position 16 nt upstream of the putative translation initiation codon of the gene *Q9H7K4* was the only specific change seen for patients with chromosome 16q22.1–linked ADCA. We renamed this protein "puratrophin-1," meaning Purkinje cell atrophy associated

The figure is available in its entirety in the online edition of *The American Journal of Human Genetics*.

Figure 5 Southern-blot analysis. The legend is available in its entirety in the online edition of *The American Journal of Human Genetics*.

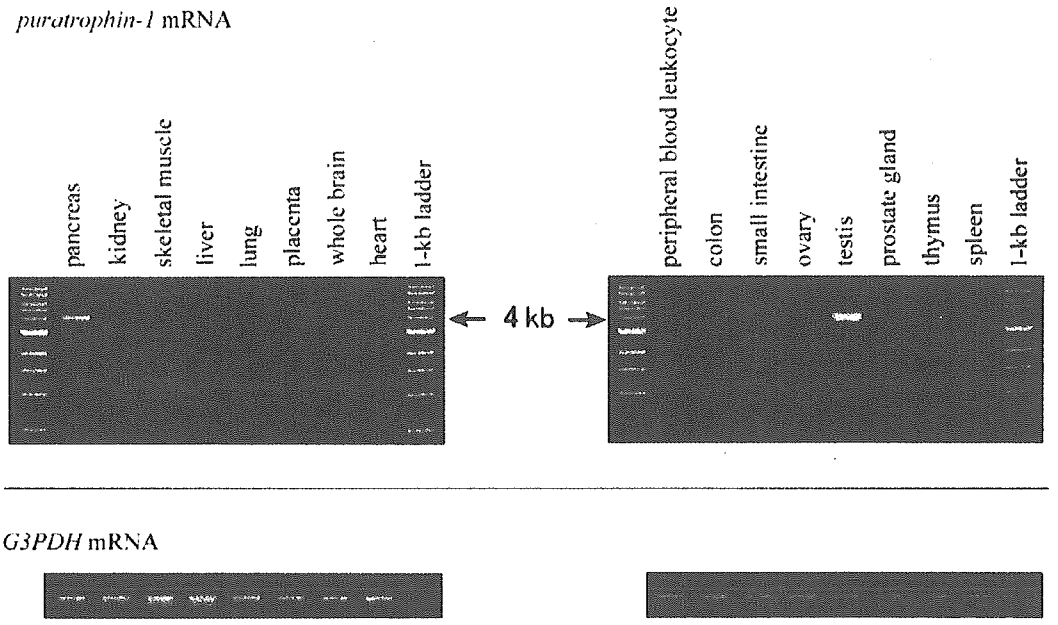

Figure 6 *Puratrophin-1* mRNA expression in various control human tissues. With this nonquantitative RT-PCR analysis, a relatively stronger expression was observed in the testis and pancreas, whereas mild or moderate expression was seen in the spleen, thymus, prostate gland, heart, placenta, lung, liver, and kidney. *Puratrophin-1* mRNA expression was low in the ovary, small intestine, colon, peripheral-blood leukocytes, whole brain, and skeletal muscle.

protein-1. (We reserved the nomenclature "ataxin-4" for families with original SCA4.)

Characterization of the Puratrophin-1 *Gene and Its Expression*

The *puratrophin-1* gene comprises 20 introns and 21 exons spanning a 13.7-kb genomic region (fig. 3*A*). RT-PCR and RACE experiments revealed that this gene is expressed in the human brain with an 8,561-nt mRNA and a single ORF of 3,576 nt (from nt 4,271 to nt 7,846) (fig. 3*B*). The first exon was 4,769 nt in length. This "full-length" transcript is predicted to encode a 134-kD protein, consisting of 1,192 aa, that contains four important domains: the cellular retinaldehyde-binding (CRAL)/triple function domain (TRIO) (at codons 304–338), the spectrin-repeat domain in the middle portion (at codons 447–601), the guanine-nucleotide exchange factor (GEF) for Rho/Rac/Cdc42-like GTPases followed by the Dbl-homologous (Rho GEF/DH) domain (at codons 733–907), and the pleckstrin-like homology (PH) domain (at codons 921–1027). The presence of these four domains suggests the role of puratrophin-1 in intracellular signaling and actin dynamics targeted to the Golgi apparatus (Godi et al. 1998; Fucini et al. 2000).

Besides the full-length *puratrophin-1* mRNA, we also found several alternative transcripts in human cerebellar cDNA (fig. 3*B*). The most common one had an unspliced intron 1 between exons 1 and 2 ("short-form" *puratrophin-1* mRNA). This intron retention produced a frameshift after exon 1 that resulted in a premature stop codon after 26 aa residues in intron 1. There were several other alternative transcripts (B1–B8 [fig. 3*B*]) in addition to full-length and short-form *puratrophin-1* mRNA. However, expression levels of these transcripts were considered lower than those of full-length or short-form *puratrophin-1* mRNA, as judged from cloning frequencies. *Puratrophin-1* mRNA was expressed in many tissues with various expression levels (fig. 6). The strongest expression was observed in the testis and pancreas, whereas its expression level was low in the "whole" brain. The expression was very weak on northern-blot analysis, even in the testis and pancreas (data available on request), which indicates that the expression of *puratrophin-1* mRNA was not abundant.

The Consequence of a C→T Change for Puratrophin-1 *mRNA Expression*

The consequence of the C→T change in the *puratrophin-1* gene was assessed by RT-PCR on frozen cerebellar tissues of two patients. No aberrant *puratrophin-1* mRNA was detected, which indicates that the mutation in the 5′ UTR does not affect alternative transcrip-

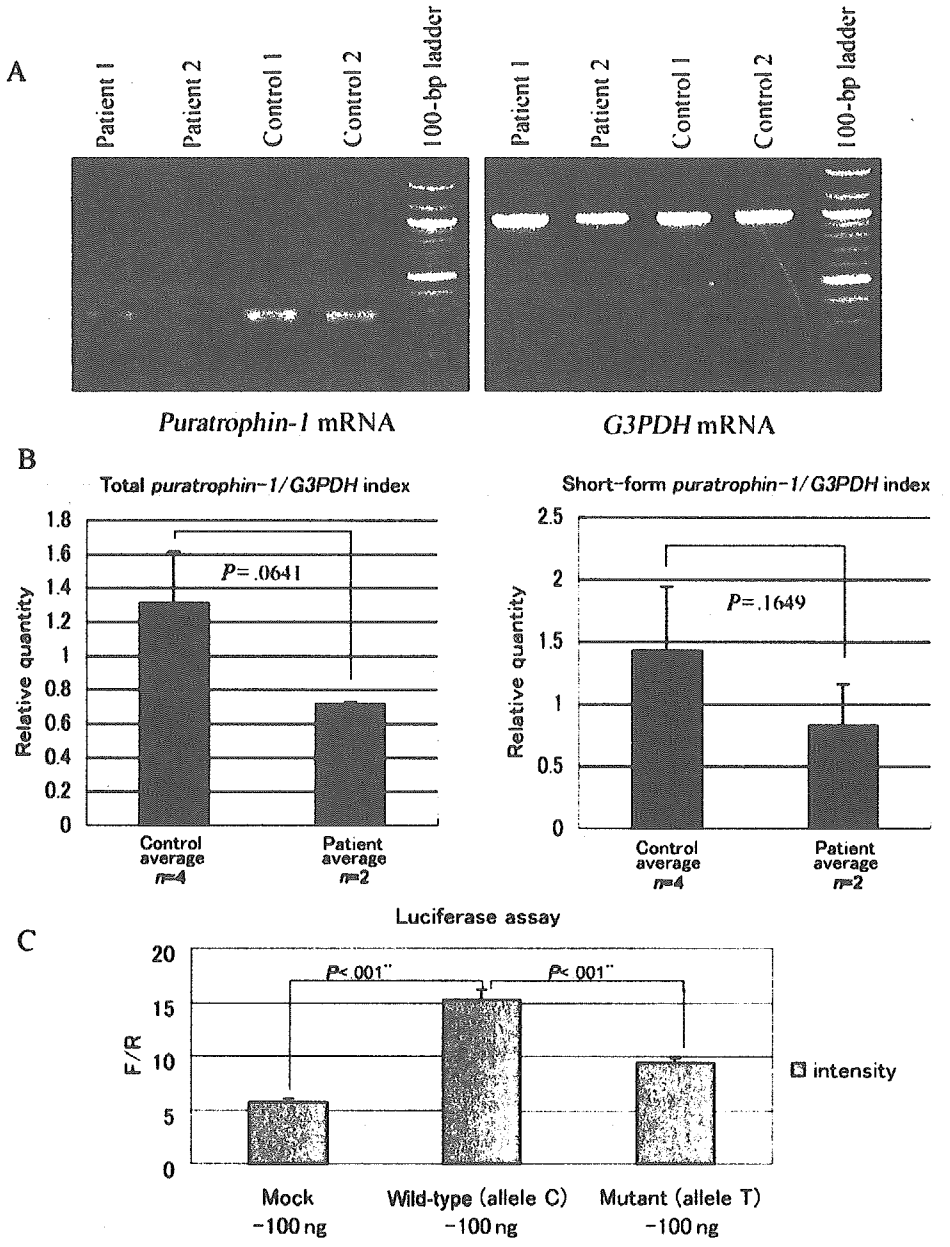

Figure 7 The consequence of a C→T change in the 5′ UTR of *puratrophin-1* mRNA. *A*, The *puratrophin-1* mRNA level assessed relative to *G3PDH* mRNA levels. The *puratrophin-1* mRNA levels in the cerebella of individuals with chromosome 16q22.1–linked ADCA appear slightly decreased compared with levels in control individuals. *B*, Quantitative analysis of *puratrophin-1* mRNA, with the use of the TaqMan technique in cerebellar mRNAs of four control individuals (with AD) and of two individuals with chromosome 16q22.1–linked ADCA. Both total *puratrophin-1* mRNA (i.e., full-length and short-form mRNAs) and short-form *puratrophin-1* mRNAs tended to be reduced in cerebella of individuals with chromosome 16q22.1–linked ADCA, although the significance was not statistically proven ($P = .0641$ for total mRNA; $P = .1649$ for short-form mRNA). *C*, Histogram of in vivo luciferase assay. "F/R" denotes fire-fly luciferase activity versus Renilla activity. The wild-type construct with allele C increases luciferase expression compared with an empty vector (Mock), whereas the mutant construct with allele T demonstrates significantly reduced luciferase activity ($P < .001$).